

# **Dark Matter in Compact Objects (TBD)**

Michael Virgato  
0000-0002-8396-0896

Submitted in total fulfilment  
of the requirements of the degree of

Doctor of Philosophy

School of Physics  
The University of Melbourne

XXX XXX

Produced on archival quality paper.

Copyright © XXX Michael Virgato

All rights reserved. No part of the publication may be reproduced in any form by print, photoprint, microfilm or any other means without written permission from the author.

# **Abstract**

DM in COs Heat up Maybe See



# Publications

Refs. [1–6] below are the journal publications, and preprints authored or co-authored during my PhD candidature. The authors are listed alphabetically in all of the titles.

## Journal papers and preprints

- [1] Papers



# **Declaration**

This is to certify that

1. the thesis comprises only my original work towards the PhD except where indicated in the preface;
2. due acknowledgement has been made in the text to all other material used;
3. the thesis is less than 100,000 words in length, exclusive of tables, maps, bibliographies and appendices.

---

Michael Virgato, XXX XXX



# Preface

We don't know what DM is. Can NSs constrain it?



# Acknowledgements

Why did I do this?



# Contents

<b>List of Figures</b>	<b>xv</b>
<b>List of Tables</b>	<b>xvii</b>
<b>1 Introduction</b>	<b>1</b>
1.1 Evidence for Dark Matter . . . . .	1
1.1.1 Astrophysical Observations . . . . .	1
1.1.2 Cosmological Evidence . . . . .	3
1.2 Potential Models of Dark Matter . . . . .	5
1.2.1 Dark Matter in an Effective Fields Theory Framework . . . . .	8
1.2.2 Overview of Effective Field Theory . . . . .	8
1.2.3 Dimension 6 EFT Operators for Dirac Fermion Dark Matter	9
1.2.4 Going from DM-Quark to DM-Nucleon Interactions . . . . .	9
1.3 Current Status of Dark Matter Constraints . . . . .	12
1.3.1 Collider Bounds . . . . .	12
1.3.2 Direct Detection Searches . . . . .	13
1.3.3 Indirect Detection . . . . .	16
1.4 Compact Objects as Dark Matter Probes . . . . .	18
<b>2 A Primer on Compact Objects</b>	<b>21</b>
2.1 Structure Equations from General Relativity . . . . .	22
2.2 White Dwarfs . . . . .	25
2.2.1 The FMT Equation of State . . . . .	25
2.2.2 Observational Status . . . . .	30
2.3 Neutron Stars . . . . .	30
2.3.1 Observational Status . . . . .	33
<b>3 Capture Part 1: Point Like Targets</b>	<b>35</b>
3.1 Dark Matter Capture in the Sun . . . . .	35
3.2 Capture in Compact Objects . . . . .	38
3.2.1 General Relativistic Corrections to the Capture Rate . . . . .	39
3.2.2 Interaction Rate for Degenerate Targets . . . . .	41

3.3	White Dwarfs: Electron Targets . . . . .	41
3.4	Neutron Stars: Leptoinc Targets . . . . .	41
<b>4</b>	<b>Capture Rate for Strongly Interacting Baryonic Matter</b>	<b>43</b>
<b>5</b>	<b>Dark Matter Induced Heating of Neutron Stars</b>	<b>45</b>
5.1	Thermalisation Time . . . . .	45
5.2	Capture-Annihilation Equilibrium . . . . .	45
5.3	Dark Matter Heating . . . . .	45
5.3.1	Kinetic Heating . . . . .	45
5.3.2	Annihilation Heating . . . . .	45
<b>6</b>	<b>Conclusion</b>	<b>47</b>
<b>Appendix A Kinematics</b>		<b>49</b>
<b>Appendix B Kinetic Heating</b>		<b>51</b>
B.1	DM Orbits in General Isometric Metric . . . . .	51
B.2	Procedure for calculating kinetic heating time . . . . .	53
<b>Definition of Symbols and Abbreviations</b>		<b>55</b>

# List of Figures

1.1	Galaxy rotation curve for NGC 6503, showing the contributions to the total velocity (red) from the DM halo (blue), disk (yellow), and gas components. Data used in making this plot was obtained from [8, 9].	3
1.2	Image of the Bullet Cluster with contours of the gravitational potential superposed. The red regions indicate the baryonic matter after the collision, while the purple regions are the expected DM components deduced from gravitational lensing. <b>cite</b>	4
1.3	Illustrative landscape of dark matter models and the mass range for which they predict a valid candidate.	6
1.4	Current status of direct detection searches for dark matter. <b>Top:</b> Spin-independent dark matter-nucleon scattering. <b>Bottom:</b> Spin-dependent dark matter-proton scattering.	14
1.5	Limits on the SD dark matter-proton cross-section from the IceCube collaboration assuming 100% branching fraction to $b\bar{b}$ (red), $W^+W^-$ (blue) or $\tau^+\tau^-$ (orange) final states. Also shown is the result from the PICO-2L DD experiment. This plot was recreated with data taken from Ref. [73].	17
1.6	Illustration of DM-induced heating of compact objects. <b>Left:</b> kinetic heating due to DM scattering, raising the temperature to $\sim 1700$ K. <b>Right:</b> Annihilation heating contributes an additional $\sim 800$ K. This image is inspired by Ref. [127].	19
2.1	Electron number density (top left), chemical potential (top right), and escape velocity (bottom) radial profiles for the carbon WDs with FMT EoS in Table 2.1. The radial distance of each profile has been normalised to the radius of the star.	29
2.2	Mass-Radius relation of WDs calculated from the FMT EoS in the zero temperature approximation (dark blue), at $10^5$ K (yellow), $10^7$ K (orange), and $10^8$ K (red), together with observed WDs from Gaia EDR2 observations [143] (light blue dots).	31

3.1 Geometry of the capture process. The azimuthal angles are not shown for simplicity as they can be integrated over trivially. . . . . 37

# List of Tables

1.1	Dimension 6 EFT operators [30] for the coupling of Dirac DM to fermions (column 2), together with the squared matrix elements DM-fermion scattering (column 5), where $s$ and $t$ are Mandelstam variables, $\mu = m_\chi/m_T$ , and $m_T$ is the target mass. . . . .	10
2.1	Four configurations for white dwarfs composed of carbon, with an FMT EoS. Shown are the central densities, $\rho_c$ , stellar mass $M_\star$ and radius $R_\star$ , and escape velocity at the edge of the WD, $v_{\text{esc}}$ . . . . .	28



# 1

## Introduction

Dark Matter is an enigma in modern physics. Despite the significant scientific effort that has gone into trying to discern its nature, a definitive detection proving its existence eludes us. Nevertheless, dark matter's influence on our Universe is undeniable, with evidence supporting its existence arising on **all** scales, large and small.

### 1.1 Evidence for Dark Matter

Today, the amount of evidence in support of dark matter's existence is overwhelming. This evidence comes from astrophysical and cosmological observations inconsistent with a universe composed entirely of visible matter. This section serves as a review of this evidence.

#### 1.1.1 Astrophysical Observations

##### Galaxy Clusters

Some of the first hints of dark matter's existence came from observations of galaxy clusters. Perhaps the most famous analysis was performed by Fritz Zwicky [7], who was puzzled by the high rotational velocities of galaxies within the Coma Cluster. By applying the virial theorem, equating the cluster's kinetic and gravitational potential energies, he found that the cluster would need to contain a much more significant amount of *dunkle materie* (dark matter) than visible matter to accommodate these high velocities.

## Rotation Curves of Spiral Galaxies

The anomalous rotational velocities observed in galaxy clusters can also be observed at the galactic scale. The rotation curves of spiral galaxies, which relate the rotational velocities of stars to their distance from the galactic centre, were observed to be flat at large distances. From the observed distribution of visible matter, Newtonian mechanics predicts that the orbital velocity of a star a distance  $r$  from the galactic centre,  $v_*(r)$ , is related to the mass of the galaxy,  $M(r)$ , through

$$v_*(r) = \sqrt{\frac{GM(r)}{r}}, \quad (1.1)$$

indicating that the velocity should fall off as  $1/\sqrt{r}$  at the outer regions of the galaxy where  $M(r)$  is constant. Instead, observations of many spiral galaxies indicate that this velocity remains constant out to the galaxy's edge.

A simple way to produce such a rotation curve is to introduce a spherically symmetric distribution of dark matter around the galaxy,

$$\rho_{\text{DM}}(r) = \frac{v_0^2}{4\pi G r^2}, \quad (1.2)$$

that results in a constant rotational velocity of  $v_0$  out to the galaxy edge. Detailed simulations of structure formation in a Cold Dark Matter (CDM) Universe indicate that the dark matter halo follows a Navaro-Frenk-White (NFW) profile, [cite for NFW](#)

$$\rho_{\text{DM}}(r) = \frac{\rho_0}{\left(\frac{r}{r_s}\right)\left(1 + \frac{r}{r_s}\right)^2}, \quad (1.3)$$

where  $\rho_0$  and  $r_s$  are free parameters that must be fit to each halo.

An example rotation curve for galaxy NGC 6503 is presented in Fig. 1.1, with the contributions from each of the matter components to the rotational velocity shown [8, 9]. As can be seen, the visible matter constituting disk and gas components does not explain the observed rotational velocity.

## Gravitational Lensing

As General Relativity describes, the curvature of space-time around massive entities causes light to travel along curved paths. As such, the mass of astrophysical structures can be deduced from the extent to which objects in the background are gravitationally lensed. The disparity between the mass obtained from gravitational lensing and the mass of visible matter in the system is further evidence of dark matter's existence.

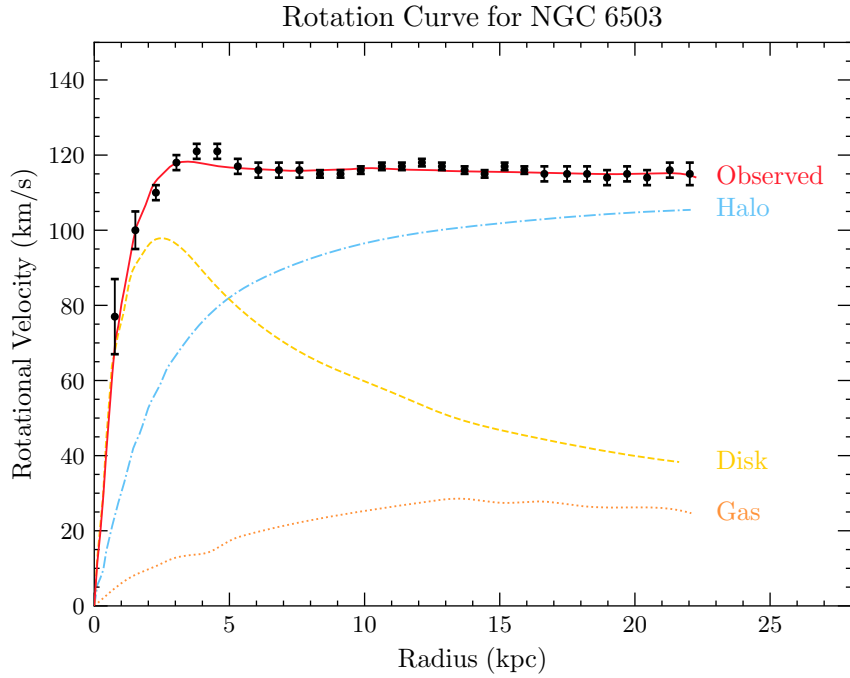


**Figure 1.1:** Galaxy rotation curve for NGC 6503, showing the contributions to the total velocity (red) from the DM halo (blue), disk (yellow), and gas components. Data used in making this plot was obtained from [8, 9].

### The Bullet Cluster

The bullet cluster is the result of two colliding galaxy clusters which the Chandra X-ray telescope imaged. When viewed in the X-ray, the smearing of the visible matter after the collision is clearly seen, as shown in the red regions of Fig. 1.2, which is expected from such a collision. However, when the gravitational potential was mapped using gravitational lensing, it was clear that the majority of the mass was displaced relative to the visible matter. This mass is attributed to the dark matter components of the original clusters. As indicated by the purple regions in Fig. 1.2, the dark matter halos seem to have passed through each other mostly unperturbed. This tells us that not only is the majority of the mass comprised of dark matter, but that the dark matter has extremely small interactions with both the visible matter and itself.

#### 1.1.2 Cosmological Evidence

Dark matter has played a major role in the cosmological history of our Universe. The current best cosmological model is the  $\Lambda$ -Cold Dark Matter model ( $\Lambda$ CDM), in



**Figure 1.2:** Image of the Bullet Cluster with contours of the gravitational potential superposed. The red regions indicate the baryonic matter after the collision, while the purple regions are the expected DM components deduced from gravitational lensing. [cite](#)

which cold (i.e. non-relativistic) dark matter plays a prominent role. The relative amount of dark matter present in our Universe can be determined with measurements of the light element abundances produced via Big Bang Nucleosynthesis (BBN).

### The Cosmic Microwave Background

One of the best probes of cosmological models is the Cosmic Microwave Background (CMB). The CMB is the radiation that was emitted during recombination when the Universe had cooled enough for electrons and protons to combine and not be ionised by the photon bath. While the CMB temperature looks isotropic on large scales, fluctuations around the average value of  $T_{\text{CMB}} \sim 2.73 \text{ K}$  are observed at very small scales. These anisotropies are the result of oscillations in the baryonic matter known as Baryon Acoustic Oscillations (BAO). These oscillations were produced due to the interplay between the outward pressure caused by matter interactions and the pull of gravitation due to dark matter.

Measuring the angular power spectra of these anisotropies and fitting the cosmological parameters of the  $\Lambda$ CDM model tell us how the Universe's energy density

$(\Omega_{\text{total}})$ , is partitioned between the matter ( $\Omega_m$ ), radiation ( $\Omega_{\text{rad}}$ ), and dark energy ( $\Omega_\Lambda$ ) components. In a flat universe, of which we believe ours to be, these components should sum to  $\Omega_{\text{tot}} = 1$ . The Planck collaboration most recently performed a precise measurement of the CMB power spectrum in 2018, obtaining best-fit parameters

$$\Omega_m = 0.311 \pm 0.006, \quad \Omega_\Lambda = 0.689 \pm 0.006. \quad (1.4)$$

Combining the predicted baryon density from BBN with the CMB observations breaks down the matter abundance into the dark ( $\Omega_{\text{DM}}$ ) and baryonic ( $\Omega_b$ ) components yielding

$$\Omega_{\text{DM}} h^2 = 0.1193 \pm 0.0009, \quad \Omega_{\text{DM}} h^2 = 0.02242 \pm 0.00014, \quad (1.5)$$

where  $h$  is the dimensionless Hubble constant such that the Hubble parameter today is  $H_0 = 100 h \text{ km s}^{-1} \text{ Mpc}$ .

### Large Scale Structure

After recombination, the pressure on the baryonic matter from photons subsided, allowing the small density perturbations to grow. This would lead to the growth of stars, galaxies, and the large-scale structure we observe today [10]. N-body simulations of the Universe's evolution require a cold dark matter component for this structure to form. While a small component of the dark matter can be warm, hot dark matter would wash out small-scale structures [11].

## 1.2 Potential Models of Dark Matter

The general consensus amongst physicists is that dark matter has a particle nature, similar to the visible matter of the Standard Model. Models may be as simple as dark matter being described by a single field or there could be an extensive hidden sector with complicated symmetry structures. Given the few details we know about dark matter, there exists an enormous library of models that can produce a viable dark matter candidate. However, there are generic properties a good dark matter candidate must satisfy, namely:

- **Stable on Cosmological Timescales:** Dark matter must either be stable or have a lifetime significantly longer than the age of the Universe in order to be present in its current abundance.

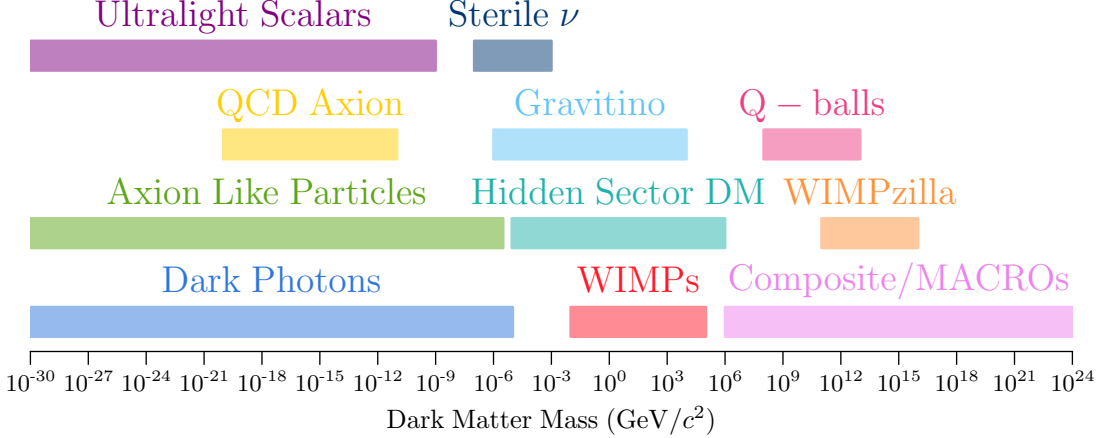


**Figure 1.3:** Illustrative landscape of dark matter models and the mass range for which they predict a valid candidate.

- **Neutral or milli-charged under Electromagnetism:** Dark matter, as its name suggests, does not significantly interact with light. By requiring that dark matter be completely decoupled from the Standard Model plasma by the time of recombination yields an upper bound on the milli-charge dark matter can carry of [12]

$$q_{\text{DM}}/e < \begin{cases} 3.5 \times 10^{-7} \left(\frac{m_{\text{DM}}}{1 \text{ GeV}}\right)^{0.58}, & m_{\text{DM}} > 1 \text{ GeV} \\ 4.0 \times 10^{-7} \left(\frac{m_{\text{DM}}}{1 \text{ GeV}}\right)^{0.35}, & m_{\text{DM}} < 1 \text{ GeV}, \end{cases} \quad (1.6)$$

- **Small Self-Interactions:** The standard  $\Lambda$ CDM cosmology assumes that the dark matter is collisionless. However, small dark matter self-interactions can help resolve existing small-scale structure issues [13, 14]. Current limits on the self-interaction cross section are  $\sigma_{\text{DM-DM}}/m_{\text{DM}} < 0.48 \text{ cm}^2/\text{g}$  come from merging galaxy clusters [15] and the ellipticity of galaxies obtained from X-ray observations [16].

A selection of the more prominent dark matter candidates is shown in Fig. 1.3. The key features of a few of these models are discussed below.

## WIMPs

The Weakly Interacting Massive Particle (WIMP) is perhaps the most well-known dark matter candidate. WIMPs rose to fame thanks to the so-called “WIMP miracle” [17]. This refers to the fact that particles with weak scale masses and annihilation cross sections just so happen to have the correct relic abundance of dark

matter when produced via the freeze-out mechanism [18]. In this scenario, the final WIMP abundance depends on the total annihilation cross-section,  $\langle\sigma v\rangle$ , with only a very mild dependence on the DM mass [19],

$$\Omega_{\text{DM}} h^2 \sim 0.12 \left( \frac{2.2 \times 10^{-26} \text{ cm}^3 \text{ s}^{-1}}{\langle\sigma v\rangle} \right). \quad (1.7)$$

The canonical weak-scale WIMP has been tightly constrained from direct and indirect detection limits, leading it to be disfavoured as a dark matter candidate. The term “WIMP” is now typically used to refer to any particle dark matter candidate that is produced thermally in the early Universe. Such a particle can have a mass in the range  $10 \text{ MeV} \lesssim m_{\text{WIMP}} \gtrsim 100 \text{ TeV}$ . Lighter WIMPs will have non-negligible contributions to the effective number of neutrino species,  $N_{\text{eff}}$ , which is constrained through BBN and the Cosmic Microwave Background CMB to be  $N_{\text{eff}} = 2.99 \pm 0.17$  [20]. Masses larger than  $\sim 100 \text{ TeV}$  are excluded from partial wave unitarity [21].

## Axions

The original axion was proposed by Peccei and Quinn [22] as part of a dynamical solution to the “Strong CP Problem”. This refers to the measured value of the neutron electric dipole moment (nEDM) being anomalously small, with a current upper bound of  $|d_n| < 0.18 \times 10^{-26} e \text{ cm}$  [23]. This can be translated to an upper bound on the CP-violating QCD  $\theta$ -parameter such that  $|\theta_{\text{QCD}}| \lesssim 10^{-10}$ , raising questions as to why this value seems to be fine-tuned to such a small value.

The Peccei-Quinn solution to this problem introduces a new, anomalous, global  $U(1)_{\text{PQ}}$  symmetry and promotes  $\theta_{\text{QCD}}$  to be a dynamical field. The axion emerges as the pseudo-Goldstone boson associated with the breaking of  $U(1)_{\text{PQ}}$ , such is in the two most prominent UV completions of the axion, the KSVZ [24, 25] and DFSZ [26, 27] models. In these models, the axion produced in the early Universe can serve the role of cold dark matter today. This makes it a very compelling dark matter candidate, as it solves two of the biggest mysteries of physics in one neat package.

However, solving the Strong CP problem can be rather restrictive on the model parameters. For example, the QCD axion’s coupling to the photon is not a free parameter and depends on the scale at which the PQ symmetry is broken. Many models introduce a light pseudoscalar particle that is not associated with a solution to the Strong CP problem but has a coupling to the photon that takes the same form as the QCD axion. Such pseudoscalars are known as “Axion Like Particles” (ALPs) and can similarly make a good dark matter candidate.

[Add some more candidates](#)

### 1.2.1 Dark Matter in an Effective Fields Theory Framework

### 1.2.2 Overview of Effective Field Theory

Given the sheer quantity of potential dark matter models and candidates, a model-independent approach for analysing experimental results is often desired. An economic analysis method is to use an Effective Field Theory (EFT) to describe the dark matter-Standard Model interactions. Effective theories are prevalent in all of physics, e.g., describing light using ray optics vs Maxwell's equations or the orbits of planets using Newtonian gravity vs General relativity. The delineating factor in choosing a formalism is the scale (energy, length, etc.) we are interested in. **Add in the usual EFT diagram** Experiments will only be sensitive to interactions that can occur below some energy scale, i.e. 13.6 TeV at the LHC or 1 GeV in direct detection experiments; we are only interested in describing the interactions that occur below this scale.

One follows two main schools of thought when constructing an EFT. First, there is the *top-down* approach. Here, you begin with a particular complete model in mind that consists of heavy and light fields. At energies below the production threshold of the heavy fields, these degrees of freedom can be “integrated out” of the theory. This process leaves an effective theory for the interactions amongst the light fields. The interactions that would be mediated by the heavy fields appear as non-renormalisable operators that are suppressed by this high energy scale,  $\Lambda$ .

The second method, known as the *bottom-up* approach, is more agnostic to the high-energy physics that might be in play. In this method, one constructs all possible operators that obey the required symmetries of the theory up to a desired mass dimension. Operators of mass dimension greater than four are then suppressed by powers the required number of powers of the high energy cutoff scale,  $\Lambda$ . This cutoff scale indicates the energy at which the EFT begins to break down and should at least be larger than the masses of the fields in the EFT. The Lagrangian constructed in this manner is made out of a tower of operators,  $\mathcal{O}_i^{(n)}$ , forming

$$\mathcal{L}_{\text{EFT}} \supset \sum_{n>4} \sum_{i=1}^{j_n} \frac{C_i^{(n)}}{\Lambda^{n-4}} \mathcal{O}_i^{(n)}, \quad (1.8)$$

where we sum over all  $j_n$  operators present at mass dimension  $n$ . The  $C_i^{(n)}$  are called Wilson coefficients and are typically energy dependent.

In the context of dark matter, there are many EFTs describing the interaction at various energy scales. For example, dark matter scattering off nuclei in direct detection experiments is described by a non-relativistic EFT built out of the momentum transfer, relative velocity and spin operators of the dark matter and targets [28,

[29]. At higher energy scales where relativistic effects become important, the EFT is instead constructed from relativistic fields, such as dark matter that may be produced in colliders.

Generally, an EFT will have fewer free parameters than the underlying UV theories, typically the dark matter mass and the high energy cutoff scale. This is in contrast with the dozens or so parameters often present in complete models. This allows for a simpler interpretation of experimental results as you will be fitting to a lower dimensional parameter space.

[Move the next sections later?](#)

### 1.2.3 Dimension 6 EFT Operators for Dirac Fermion Dark Matter

This work's approach will focus on dimension 6 EFT operators that describe the interactions of Dirac fermion dark matter with standard model fermions. These operators will have a structure

$$\mathcal{L}_{\text{EFT}}^{(6)} \sim \frac{1}{\Lambda^2} (\bar{\chi} \Gamma_{\text{DM}} \chi) (\bar{f} \Gamma_{\text{SM}} f), \quad (1.9)$$

where the  $\Gamma_i$  determines the Lorentz structure of the interaction by taking appropriate combinations from the set

$$\Gamma_i \in \{1, i\gamma_5, \gamma^\mu, i\gamma^\mu\gamma^5, \sigma^{\mu\nu}, i\sigma^{\mu\nu}\gamma^5\}. \quad (1.10)$$

For example, the case of  $\Gamma_\chi = \Gamma_{\text{SM}} = 1$  yields scalar currents for both the DM and SM fermions and would correspond to integrating out a heavy scalar mediator in the UV theory. There are 10 such operators at dimension six that form a linearly independent basis. These are given in Table 1.1, along with spin-averaged squared matrix element for dark matter scattering with a fermion. The coupling constants,  $g_f$ , are given in terms of the fermion Yukawa couplings,  $y_f$ , and the EFT cutoff scale,  $\Lambda_f$ . Hence, these operators describe interactions between dark matter and the elementary fermions of the Standard Model: the leptons and quarks.

### 1.2.4 Going from DM-Quark to DM-Nucleon Interactions

The operators in Table 1.1 describe dark matter interactions at the quark level, as these are the degrees of freedom most models are formulated with. However, we will primarily be interested in dark matter scattering with baryons, which requires taking the matrix element of the quark operators between baryon states,

Name	Operator	$g_f$	$ \bar{M}(s, t, m_i) ^2$
D1	$\bar{\chi}\chi \bar{f}f$	$\frac{y_f}{\Lambda_f^2}$	$g_f^2 \frac{(4m_\chi^2 - t)(4m_\chi^2 - \mu^2 t)}{\mu^2}$
D2	$\bar{\chi}\gamma^5\chi \bar{f}f$	$i \frac{y_f}{\Lambda_f^2}$	$g_f^2 \frac{t(\mu^2 t - 4m_\chi^2)}{\mu^2}$
D3	$\bar{\chi}\chi \bar{f}\gamma^5 f$	$i \frac{y_f}{\Lambda_f^2}$	$g_f^2 t (t - 4m_\chi^2)$
D4	$\bar{\chi}\gamma^5\chi \bar{f}\gamma^5 f$	$\frac{y_f}{\Lambda_f^2}$	$g_f^2 t^2$
D5	$\bar{\chi}\gamma_\mu\chi \bar{f}\gamma^\mu f$	$\frac{1}{\Lambda_f^2}$	$2g_f^2 \frac{2(\mu^2 + 1)^2 m_\chi^4 - 4(\mu^2 + 1)\mu^2 s m_\chi^2 + \mu^4 (2s^2 + 2st + t^2)}{\mu^4}$
D6	$\bar{\chi}\gamma_\mu\gamma^5\chi \bar{f}\gamma^\mu f$	$\frac{1}{\Lambda_f^2}$	$2g_f^2 \frac{2(\mu^2 - 1)^2 m_\chi^4 - 4\mu^2 m_\chi^2 (\mu^2 s + s + \mu^2 t) + \mu^4 (2s^2 + 2st + t^2)}{\mu^4}$
D7	$\bar{\chi}\gamma_\mu\chi \bar{f}\gamma^\mu\gamma^5 f$	$\frac{1}{\Lambda_f^2}$	$2g_f^2 \frac{2(\mu^2 - 1)^2 m_\chi^4 - 4\mu^2 m_\chi^2 (\mu^2 s + s + t) + \mu^4 (2s^2 + 2st + t^2)}{\mu^4}$
D8	$\bar{\chi}\gamma_\mu\gamma^5\chi \bar{f}\gamma^\mu\gamma^5 f$	$\frac{1}{\Lambda_f^2}$	$2g_f^2 \frac{2(\mu^4 + 10\mu^2 + 1)m_\chi^4 - 4(\mu^2 + 1)\mu^2 m_\chi^2 (s + t) + \mu^4 (2s^2 + 2st + t^2)}{\mu^4}$
D9	$\bar{\chi}\sigma_{\mu\nu}\chi \bar{f}\sigma^{\mu\nu} f$	$\frac{1}{\Lambda_f^2}$	$8g_f^2 \frac{4(\mu^4 + 4\mu^2 + 1)m_\chi^4 - 2(\mu^2 + 1)\mu^2 m_\chi^2 (4s + t) + \mu^4 (2s + t)^2}{\mu^4}$
D10	$\bar{\chi}\sigma_{\mu\nu}\gamma^5\chi \bar{f}\sigma^{\mu\nu} f$	$\frac{i}{\Lambda_f^2}$	$8g_f^2 \frac{4(\mu^2 - 1)^2 m_\chi^4 - 2(\mu^2 + 1)\mu^2 m_\chi^2 (4s + t) + \mu^4 (2s + t)^2}{\mu^4}$

**Table 1.1:** Dimension 6 EFT operators [30] for the coupling of Dirac DM to fermions (column 2), together with the squared matrix elements DM-fermion scattering (column 5), where  $s$  and  $t$  are Mandelstam variables,  $\mu = m_\chi/m_T$ , and  $m_T$  is the target mass.

i.e.  $\langle \mathcal{B} | \bar{q} \Gamma_q q | \mathcal{B} \rangle$ . These matrix elements can be calculated through the application of Chiral Perturbation Theory (ChPT), giving a baryon level EFT. The operators of this EFT will have the same form as those in Table 1.1, with the obvious replacement of  $f \rightarrow \mathcal{B}$ , as well as additional form factors that take into account the structure of the baryons.

The required form factors for each operator have been calculated at zero mo-

momentum transfer in Ref. [28] and are given by

$$c_{\mathcal{B}}^S(0) = \frac{2m_{\mathcal{B}}^2}{v^2} \left[ \sum_{q=u,d,s} f_{T_q}^{(\mathcal{B})} + \frac{2}{9} f_{T_G}^{(\mathcal{B})} \right]^2, \quad (1.11)$$

$$c_{\mathcal{B}}^P(0) = \frac{2m_{\mathcal{B}}^2}{v^2} \left[ \sum_{q=u,d,s} \left( 1 - 3 \frac{\bar{m}}{m_q} \right) \Delta_q^{(\mathcal{B})} \right]^2, \quad (1.12)$$

$$c_{\mathcal{B}}^V(0) = 9, \quad (1.13)$$

$$c_{\mathcal{B}}^A(0) = \left[ \sum_{q=u,d,s} \Delta_q^{(\mathcal{B})} \right]^2, \quad (1.14)$$

$$c_{\mathcal{B}}^T(0) = \left[ \sum_{q=u,d,s} \delta_q^{(\mathcal{B})} \right]^2, \quad (1.15)$$

where  $v = 246$  GeV is the vacuum expectation value of the SM Higgs field,  $\mathcal{B}$  is the baryonic species,  $\bar{m} \equiv (1/m_u + 1/m_d + 1/m_s)^{-1}$  and  $f_{T_q}^{(\mathcal{B})}$ ,  $f_{T_G}^{(\mathcal{B})} = 1 - \sum_{q=u,d,s} f_{T_q}^{(\mathcal{B})}$ ,  $\Delta_q^{(\mathcal{B})}$  and  $\delta_q^{(\mathcal{B})}$  are the hadronic matrix elements, determined either experimentally or by lattice QCD simulations<sup>1</sup>. The specific values of these matrix elements for various baryons are provided in Appendix ADD APPENDIX.

These form factors are perfectly viable when considering interactions with momentum transfers  $\lesssim 1$  GeV such as in direct detection experiments. For energies greater than this, the internal structure of the baryon begins to be resolved, and an additional momentum-dependent form factor is required to account for this [31],

$$F_{\mathcal{B}}(t) = \frac{1}{(1 - t/Q_0)^2}, \quad (1.16)$$

where  $t$  is the Mandelstam variable, and  $Q_0$  is an energy scale that depends on the hadronic form factor. For simplicity, we will conservatively take  $Q_0 = 1$  GeV for all operators. Putting everything together, the squared coupling constants for dark matter-baryon interactions are obtained by making the replacement

$$g_f^2 \rightarrow \frac{c_{\mathcal{B}}^I(t)}{\Lambda_q^4} \equiv \frac{1}{\Lambda_q^4} c_{\mathcal{B}}^I(0) F_{\mathcal{B}}^2(t), \quad I \in S, P, V, A, T, \quad (1.17)$$

in the matrix elements in the final column of Table 1.1.

---

<sup>1</sup>The superscript letters  $S$ ,  $P$ ,  $V$ ,  $A$  and  $T$  stand for Scalar, Pseudoscalar, Vector, Axial-vector and Tensor interactions respectively. The corresponding operators are: D1-2 for  $S$ ; D3-4 for  $P$ ; D5-6 for  $V$ , D7-8 for  $A$ ; and D9-10 for  $T$ .

## 1.3 Current Status of Dark Matter Constraints

In broad terms, there are three main ways that we can search for evidence of dark matter, often termed “make it, shake it or break it”. “Make it” refers to dark matter being produced at colliders; “break it” to searching for dark matter annihilation signals; and “shake it” to direct detection of dark matter scattering. An illustrative way of depicting these processes is shown in Fig. [add usual diagram](#). This section discusses the current status of these detection methods.

### 1.3.1 Collider Bounds

If dark matter is produced in a collider, it will simply leave the detector without depositing any energy. In order to determine if such an invisible particle was produced, conservation of energy-momentum is used to determine if there are any events that are missing energy. In practice, what is searched for is missing momentum that is transverse to the beamline.

Currently, dark matter has not been observed to be produced in particle colliders. This non-observation has instead been used to constrain the dark matter mass and production cross sections or couplings of various models. These limits are typically interpreted in a model-dependent manner, as different dark matter - Standard model couplings can significantly alter the production rates. As mentioned above, EFTs can be used to explore a variety of interactions in a somewhat model-independent way. However, many applications of this nature did not hold up to scrutiny, as the EFTs were being applied at energies outside their regions of validity [32–35], and so care is needed when applying such methods.

The ATLAS and CMS experiments at the LHC have performed analyses on various dark matter production mechanisms, including the exchange of a  $Z/Z'$  or Higgs, EFTs and heavy mediators, and mono-jet searches [36]<sup>2</sup>. Collider searches also offer complimentary probes of the dark matter-nucleon scattering cross-section [37].

It is important to note that an observation of an invisible massive particle at a collider is not enough to infer that it is dark matter. Such an observation only tells us that such a particle exists but nothing about its abundance, meaning it could just be a sub-component of a larger dark sector. In order to identify whether or not this was a dark matter detection, complimentary observations from direct or indirect detectors would be required.

---

<sup>2</sup>These searches refer to a single jet being produced alongside a pair of dark matter particles. This jet could be of Standard Model or dark sector origin, with the latter commonly referred to as “mono-X” searches.

### 1.3.2 Direct Detection Searches

Direct detection experiments vary wildly depending on the dark matter mass range they are trying to probe. For ALP dark matter that is wavelike, haloscope experiments such as ADMX [38] and MADMAX [39] attempt to convert ALPs to photons via the Primakoff effect. Searches for WIMP dark matter look for the dark matter scattering with some detector material, causing it to recoil and release some energy. Given our focus on WIMP dark matter, this section will review the experimental status of these detectors.

The differential rate at which the incoming flux of dark matter will scatter within a detector with  $N_T$  targets, as a function of the recoil energy,  $E_R$ , is given by

$$\frac{dR(E_R, t)}{dE_R} = N_T \frac{\rho_{\text{DM}}}{m_{\text{DM}}} \int_{v > v_{\min}}^{v_{\text{esc}}} v f(\vec{v} + \vec{v}_E) \frac{d\sigma}{dE_R} d^3v, \quad (1.18)$$

and depends on the quantities:

- $v_{\min}$  is the minimum dark matter velocity required by kinematics for a scattering event to occur;
- $v_{\text{esc}} = 528 \text{ km s}^{-1}$  is the Milky Way escape velocity;
- $\vec{v}_E$  is the velocity of the Earth through the dark matter halo<sup>3</sup>;
- $f(\vec{v} - \vec{v}_E)$  is the dark matter velocity distribution in the Earth's frame;
- $d\sigma/dE_R$  is the differential scattering cross-section.

Given the low interaction rate of dark matter, the expected event rate in detectors is very low, around one event per day, per kilogram of target material, per kiloelectronvolt deposited. Having such a low event rate requires the detector to be situated in an extremely low background environment, such as underground laboratories.

Direct detection experiments aim to probe two main types of dark matter interactions: Spin-dependent (SD) and spin-independent (SI) scattering. SD interactions couple to the overall spin of the target, while SI interactions are agnostic to this. Therefore, experiments searching for SI interactions benefit from using nuclei with a large atomic number,  $A$ , as the interaction cross-section will involve a coherent sum over all nucleons. This leads to an  $A^2$  enhancement of SI interactions compared to the SD counterpart.

---

<sup>3</sup>This accounts for the orbit of the Earth around the Sun, which induces an annual modulation in the flux of DM.

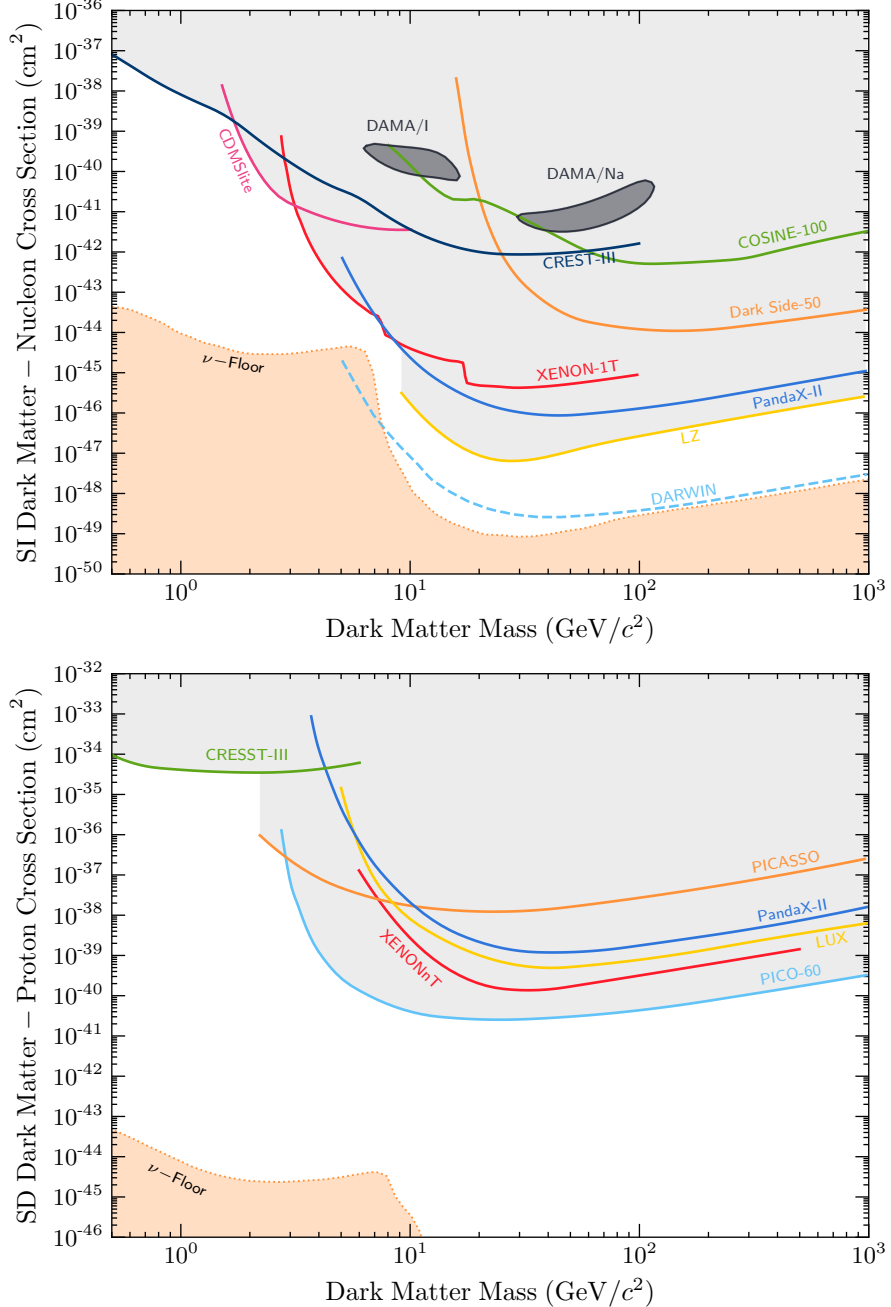


**Figure 1.4:** Current status of direct detection searches for dark matter. **Top:** Spin-independent dark matter-nucleon scattering. **Bottom:** Spin-dependent dark matter-proton scattering.

The current leading constraints on the dark matter-nucleon scattering cross-section are shown in Fig. 1.4, with SI in the top panel and SD in the bottom. The SI limits are set by liquid noble gas experiments (LZ [40], XENON-1T [41], PandaX-II [42], and DarkSide-50 [43]), solid-state cryogenic detectors (CRESST-III [44], CDMSlite [45], with projected DARWIN sensitivities [46]), and room temperature crystals (DAMA/LIBRA [47], and COSINE-100 [48]).

The SD experiments require their targets to carry non-zero spin for the dark matter to couple to.  $^{19}\text{F}$  is the favourable choice proton scattering, as it has an unpaired proton giving it its overall spin. The leading constraints come from superheated liquid experiments such as the PICO-60 [49] as well as PICASSO [50]. In terms of the SD proton scattering shown in Fig 1.4, These interactions are also searched for by many of the same experiments in the SI case, with the inclusion of LZ's predecessor LUX [51].

The orange dashed line represents the neutrino floor<sup>4</sup>, a theoretical lower limit on the discoverability of WIMP-like dark matter. In this region of parameter space, doctors will become sensitive to the irreducible background from neutrino scattering, which will produce signals almost indistinguishable from a true dark matter interaction. A significant amount of effort is being put toward overcoming this hindrance, with the main strategy being to take advantage of the directionality of dark matter flux [53].

Many experiments begin to lose sensitivity to low-mass dark matter ( $m_{\text{DM}} \lesssim 10 \text{ GeV}$ ) as the targets recoil with energies below the detector threshold. Current energy thresholds can reach as low as  $\sim \mathcal{O}(100 \text{ eV})$ , which is on the same order of magnitude as the recoil energy due to a 1 GeV dark matter collision. The sensitivity also falls off at a slower rate at larger masses, though this is due to the number of dark matter particles that pass through the detector given  $N_{\text{DM}} = \rho_{\text{DM}}/m_{\text{DM}}$ , and the dark matter density is known to be  $0.4 \text{ GeV cm}^{-3}$ .

Direct detection limits also assume that the scattering cross-section is independent of the dark matter velocity and momentum transfer in the interaction. Given that the local dark matter dispersion velocity is predicted to be  $v_d = 270 \text{ km s}^{-1} \approx 10^{-3}c$ , a back-of-the-envelope estimation for the momentum transfer gives  $q_{\text{tr}} \lesssim 100 \text{ MeV}$ . Therefore, cross-sections proportional to  $v_{\text{DM}}$  or  $q_{\text{tr}}$  will result in significantly lower event rates and hence much weaker limits than the unsuppressed interactions.

This leads us to indirect detection methods, which can provide complementary probes to direct detection while also exploring interactions that are difficult, if not impossible, for terrestrial-based detectors to observe.

---

<sup>4</sup>Calling this the “neutrino fog” rather than floor has been gaining traction in recent years [52]

### 1.3.3 Indirect Detection

Indirect detection experiments aim to infer the presence of dark matter through its annihilation or decay into Standard Model states. These searches look for anomalies in astrophysical data, though dark matter accumulating within the Earth’s core can also produce a detectable signal [54, 55]. The signals searched for include:

- Gamma-rays at terrestrial-based telescopes such as HESS [56–58], VERITAS [59–61], MAGIC [62, 63] and HAWC [64–67] as well as the Fermi-LAT [68–72] satellite;
- Neutrino signals at IceCube [73, 74], ANTARES [55, 75, 76], Super-K [77–79], and will be searched for at the upcoming Hyper-K [80–82], JUNO [83] experiments.
- Cosmic-Rays by the AMS-02 experiment [84, 85]

Signals from dark matter annihilation are best searched for by looking at regions where the dark matter density is expected to be high, boosting the annihilation rate. Natural places to look include the Galactic Centre [86, 87], dwarf-spheroidal galaxies [88], and celestial bodies where dark matter can accumulate over time. This last option is of primary interest to this work.

Stars have long been used to study various models of dark matter. ALPs of dark photons can be produced within the plasma of stars, altering the energy transport properties within them. This can ultimately lead to deviations in the evolution of the star, which can be used to place some of the strongest constraints on these models [89–91]. WIMP-like dark matter from the halo that couples to visible matter can scatter within the objects. The dark matter may lose enough energy in these interactions to become gravitationally bound to the object, leading to a population of dark matter being accumulated over time [18, 92–95].

The capture of dark matter within the Sun has been extensively studied. The formalism set up by Gould [93, 94, 96] has remained quite successful, with many authors building on these foundations over time [95, 97, 98]. The captured dark matter can thermalise within the Sun’s core, where it may annihilate and produce an observational signal. This could be via direct annihilation to neutrinos [75–77, 99, 100], or to some other long-lived state that can escape the Sun and decay into visible states [101–105]. Additionally, WIMPs can also alter the energy transport within the Sun [106–109].

In comparison to DD searches, interpretation of indirect detection data will require additional model-dependent assumptions, namely the relevant annihilation channels of the dark matter. The most general limits can be placed by assuming that the dark matter only has a single annihilation channel, i.e. it annihilates to a  $\tau^+\tau^-$  final state 100% of the time. Under these assumptions, limits on the SD dark

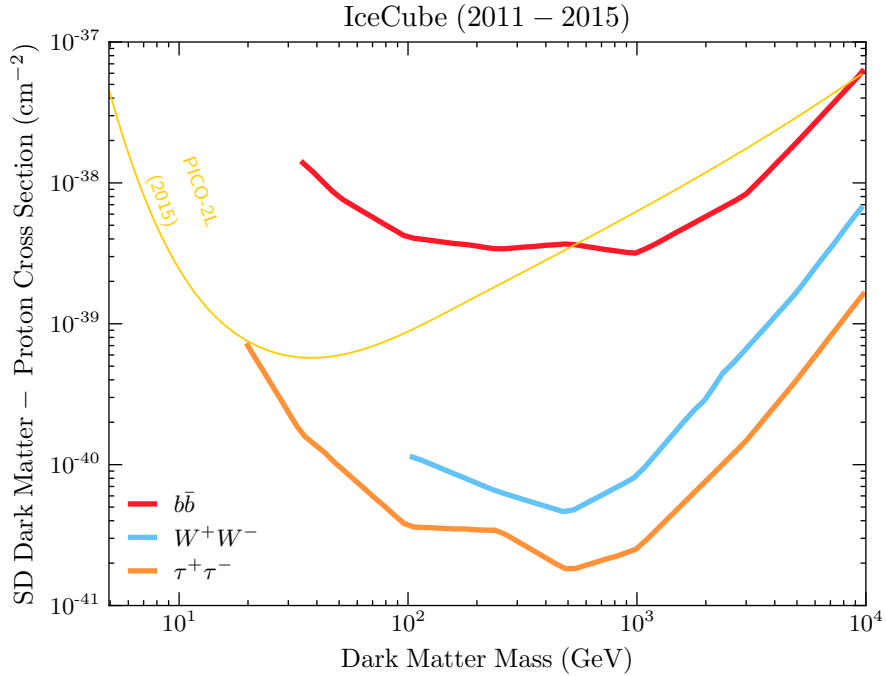


**Figure 1.5:** Limits on the SD dark matter-proton cross-section from the IceCube collaboration assuming 100% branching fraction to  $b\bar{b}$  (red),  $W^+W^-$  (blue) or  $\tau^+\tau^-$  (orange) final states. Also shown is the result from the PICO-2L DD experiment. This plot was recreated with data taken from Ref. [73].

matter-proton cross-section have been placed that exceed current DD constraints, due to the rather large abundance of Hydrogen within the Sun. Constraints from the IceCube collaboration are shown in Fig. 1.5

The smallest dark matter mass that can be probed using solar capture is determined by the evaporation mass of the Sun. Below this mass, the dark matter will be efficiently evaporated out of the Sun at the same rate it is captured, thus no annihilation can take place<sup>5</sup>. Additionally, as with direct detection, the Sun will be far less sensitive to interactions that are proportional to the velocity/momentum transfer.

Overcoming the first issue requires either a colder star or one that is much heavier. The second requires dark matter to scatter with the constituent material at relativistic energies to overcome the suppression in the cross-sections. Fortunately, there exists objects that meet all these criteria, allowing for a wider variety of dark matter models to be explored than direct detection or traditional indirect detection experiments: compact objects.

---

<sup>5</sup>A more rigorous definition of evaporation and evaporation mass will be presented later in the thesis.

## 1.4 Compact Objects as Dark Matter Probes

The main goal behind this work is to explore how compact objects can be used to probe a wide variety of dark matter interactions that terrestrial direct detection experiments are insensitive to. By compact objects, we are referring to Neutron Stars (NSs) and White Dwarfs (WDs), and not Black Holes that also fall into this category.

Compact objects offer a unique laboratory for studying dark matter and its interactions with the Standard Model in environments unachievable anywhere else in the Universe. They generate strong gravitational fields and are composed of incredibly dense matter, with NSs reaching super-nuclear densities in their central cores. The capture rate within these objects is therefore enhanced due to these properties, with benefits over solar capture including:

- **Gravitational focusing of the DM flux:** The strong gravitational field will increase the impact parameter of the infalling dark matter. This increases the effective size of the capturing body, increasing the flux of dark matter passing through it.
- **Relativistic Interaction Energies:** In general, the infalling dark matter will be accelerated to (semi-)relativistic velocities ( $\sim 0.2 - 0.7c$ ). Moreover, the stellar constituents will also have relativistic energies. As such, interactions that are momentum/velocity dependent will suffer far less suppression than in DD experiments.
- **Large Number of Targets:** The extremely high densities of these objects correspond to a considerable number of targets for scattering to occur. This allows these objects to probe very small scattering cross-sections, with NSs in particular expected to reach as low as  $\sim 10^{-45} \text{ cm}^2$ .
- **Forgot the last point....**

In the past, capture in NSs has been applied primarily in the context of sending gravitational collapse into black holes [110–116], and the modifications of NS merger rates as well as the gravitational wave signatures of these mergers [117–120]. Capture in WDs has also been considered, with a variety of different applications of the capture process [121–126].

In recent years, dark matter induced heating of NSs has reemerged as a potential detection frontier [127–134]. It was shown that dark matter could reheat old, isolated NSs in our local neighbourhood back up to temperatures that would cause them to radiate as blackbody peaked in the near-infrared. The aim is to locate the NSs with radio telescopes such as the Square-Kilometer-Array (SKA), and determine their age through their spindown rate. Once located, the star’s temperature

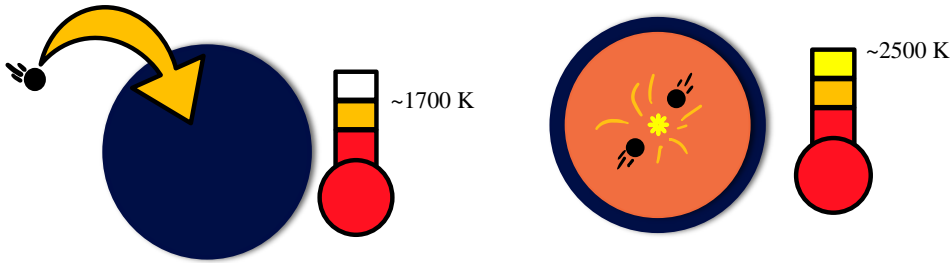


**Figure 1.6:** Illustration of DM-induced heating of compact objects. **Left:** kinetic heating due to DM scattering, raising the temperature to  $\sim 1700$  K. **Right:** Annihilation heating contributes an additional  $\sim 800$  K. This image is inspired by Ref. [127].

can be determined through observations from infrared telescopes such as the James Webb Space Telescope (JWST).

This heating occurs in two stages. The dark matter will first deposit its kinetic energy into the star through the scatterings required for capture and its subsequent thermalisation within the NS core, with this process called *kinetic heating*. If the dark matter can annihilate, it will deposit its mass energy, assuming the products are trapped within the star, termed *annihilation heating*. These processes are illustrated in Fig. 1.6. Assuming a NS in our local neighbourhood, i.e., within

In order to accurately determine the limits on dark matter interactions that such an observation could place, one first requires an accurate calculation of the capture rate. However, all previous calculations relied on the formalism set up by Gould for capture in the Sun, with only minor modifications made to accommodate the extreme nature of the compact objects.

Chapters 3 and 4 of this thesis are devoted to reformulating Gould's capture formalism to account for the physics specific to compact objects in a self-consistent manner. These include a relativistic treatment of the kinematics, using General Relativity to calculate the correct dark matter flux passing through the star, and accounting for Pauli blocking of the final state target using Fermi-Dirac statistics for the stellar constituents. In addition, we incorporate the internal structure of these objects by calculating the radial profiles for the relevant microscopic quantities (e.g., chemical potentials and number densities) via the adoption of a realistic equation of state.

Further considerations are required when considering dark matter interactions with the baryonic matter inside NSs. Due to the high density of the NS interior, the baryonic matter undergoes strong interactions amongst themselves and should not be treated as a free Fermi gas. Instead, adopting an equation of state that accounts for these interactions is required. These interactions modify the mass of the baryons, leading them to obtain an effective mass smaller than their vacuum

mass. Furthermore, as we will see, the dark matter may interact with the baryons with momentum transfers on the order of 10 GeV. This is high enough that the dark matter will begin to resolve the internal structure of the baryon. To account for this, the momentum dependence of the baryon form factors that are typically neglected in direct detection and solar capture must be reintroduced.

This formalism is made in preparation for a thorough analysis of the timescales involved in the dark matter heating of compact objects. The energy deposited in both the kinetic and annihilation heating stages does not occur instantaneously, and the timescales involved in them need to be compared to the age of the star in question. We will define kinetic heating timescale as the time required for dark matter to deposit 99% of its initial kinetic energy into the star. For annihilation heating to occur, the dark matter must reach a state of capture-annihilation equilibrium within the stellar core. In standard calculations of this timescale, the dark matter must first become thermalised with the star. Only then can annihilations occur efficiently enough to heat the star.

We will work with the EFT operators in Table 1.1 that describe Dirac fermion dark matter interacting with Standard Model leptons. Each operator will be studied in isolation, i.e., by considering a Lagrangian that contains only one of the operators rather than a linear superposition of multiple. This way, we can analyse specific types of interactions independently, allowing us to take as model-independent an approach to phenomenology as possible.

# 2

## A Primer on Compact Objects

Within the cores of stars exists a delicate balance between the gravitational force of its mass wanting to collapse in on itself, and the outward pressure generated by thermonuclear fusion of light elements. This fusion process begins with the burning of hydrogen to form helium. Eventually, the hydrogen is depleted, allowing gravity to temporarily overcome the outward pressure leading to the core contracting. As this occurs, the gravitational potential energy is converted to thermal energy and the core eventually becomes hot enough to facilitate helium burning.

This cycle continues as heavier and heavier elements are formed within the ever-increasingly hot stellar core. If the star is heavy enough, iron will eventually be formed from the burning of silicon. As the fusion of iron nuclei is an endothermic process, it will not occur spontaneously. Whatever the mass of the star, eventually it will no longer be able to support the fusion of these heavier elements. Without a sufficient fuel source, the core will collapse under its own gravity leading to the death of the star.

What comes after this depends on the mass of the progenitor stars. Very light stars,  $\lesssim 0.5M_{\odot}$ , have lifetimes much longer than the age of the universe, and so are uninteresting to our current discussion. Moderately heavy stars,  $1M_{\odot} \lesssim M_{\star} \lesssim 8M_{\odot}$ , will continue burning fuel until the outer layers of the star are dispersed as it expands, leaving a carbon-oxygen (CO) core. The core will begin to collapse until the Fermi degeneracy of the ultrarelativistic electrons is great enough to reestablish equilibrium, resulting in a White Dwarf (WD).

Heavy stars,  $\gtrsim 8M_{\odot}$ , spectacularly end their lives in a type-II supernova event. This occurs when the core of the star exceeds the Chandrasekhar mass of  $1.4M_{\odot}$ , which cannot be supported by electron degeneracy pressure. The core itself will then collapse, leading to a shockwave that ejects the majority of the mass of the star. All that will remain is an extremely dense core supported by neutron degeneracy

pressure, a Neutron Star (NS). If the star was so massive that the gravitational forces overcome even the neutron degeneracy pressure, then the core collapses into a black hole.

These three stellar corpses (white dwarfs, neutron stars, and black holes) are collectively known as compact objects, as they have masses similar to or larger than our Sun, compressed into much smaller bodies with significantly larger surface gravities. These objects do not have a source of fuel, and spend the rest of their lives cooling down. For the remainder of this thesis, we will only be interested in white dwarfs and neutron stars and refer to these collectively as compact objects, excluding black holes from this term.

This chapter is dedicated to discussing the structure and composition of these objects<sup>1</sup>.

## 2.1 Structure Equations from General Relativity

The highly dense matter comprising neutron stars and white dwarfs leads to extremely strong gravitational fields being produced by the stars. As such, modeling the structure of these objects falls into the domain of General Relativity (GR). Here we review the structure of static, spherically symmetric stars.

The assumption that the mass distribution of the star is spherically symmetric leads to the metric taking the form

$$ds^2 = -d\tau^2 = -B(r)dt^2 + A(r)dr^2 + r^2d\Omega^2, \quad (2.1)$$

with  $d\tau$  the proper time interval, and  $A(r)$ ,  $B(r)$  are functions only of the radial coordinate and are often written as

$$A(r) = e^{2\Lambda(r)}, \quad B(r) = e^{2\Phi(r)}. \quad (2.2)$$

These functions are subject to the condition that at distances far from the star space-time becomes flat, leading to the boundary conditions

$$\lim_{r \rightarrow \infty} A(r) = \lim_{r \rightarrow \infty} B(r) = 1. \quad (2.3)$$

The matter that comprises the star is modeled as a perfect fluid, meaning we are neglecting any shear stresses and energy transport within the star. Such a fluid is described by its pressure  $P(r)$ , density  $\rho(r)$ , and number density,  $n(r)$ , as well as the 4-velocity of the fluid  $u^\mu(r)$ . Being a static fluid, the only non-zero component

---

<sup>1</sup>As this work is written by a particle physicist, I wish to apologise to my astrophysics colleagues for what is to come.

of this velocity is the time component, which is fixed through  $g_{\mu\nu}u^\mu u^\nu = -1$  to be  $u^t = 1/\sqrt{B(r)}$ . These quantities are then used to construct the stress-energy tensor for the star, which takes the form

$$T^{\mu\nu} = (\rho + P)u^\mu u^\nu + Pg^{\mu\nu}. \quad (2.4)$$

The microphysics underlying the matter interactions are encoded in an equation of state (EoS) that relates the various thermodynamic quantities. This is typically given by expressing the pressure as a function of the density,  $P(\rho)$ . It is often more convenient to parameterise the EoS by the number density of baryons,  $n_b$ , and the entropy per baryon,  $s$ , such that

$$P = P(n, s), \quad \rho = \rho(n, s). \quad (2.5)$$

The dependence on  $s$  turns out to be trivial in most scenarios involving compact objects, such as those considered here. The pressure in these stars arises from the degeneracy of the nucleons in NSs or the electrons in WDs, rather than from the thermal motion of the constituents that will be frozen out at low temperatures. This is the case for temperatures much lower than the Fermi energy of the system, with typical values of  $E_F \sim 10$  MeV in NSs or  $\sim 1$  MeV in WDs, corresponding to temperatures of  $T_* \sim 10^{11}$  K and  $\sim 10^{10}$  K respectively. As these stars are expected to cool well below these temperatures quickly after formation, the entropy can be taken to be zero throughout the star. This allows us to reduce the two-parameter EoS to a simpler one-parameter one,

$$P = P(n_b, s = 0) = P(n_b), \quad \rho = \rho(n_b, s = 0) = \rho(n_b). \quad (2.6)$$

The structure of the star is therefore determined by the quantities  $A(r)$ ,  $B(r)$ ,  $P(r)$ ,  $\rho(r)$ , and  $n_b(r)$ . This system is determined by applying the Einstein field equations,  $G^{\mu\nu} = 8\pi T^{\mu\nu}$ , together with the conservation of energy-momentum,  $T^{\mu\nu}_{;\nu} = 0$ , the EoS relations Eqs. 2.6, and the appropriate boundary conditions. The structure equations that come out of this analysis were first discovered concurrently by Tolman [135] and by Oppenheimer and Volkoff [136], and so are known as the TOV equations. They take the form

$$\frac{dP}{dr} = -\rho(r)c^2 \left[ 1 + \frac{P(r)}{\rho(r)c^2} \right] \frac{d\Phi}{dr}, \quad (2.7)$$

$$\frac{d\Phi}{dr} = \frac{GM(r)}{c^2 r^2} \left[ 1 + \frac{4\pi r^3 P(r)}{M(r)c^2} \right] \left[ 1 - \frac{2GM(r)}{c^2 r} \right]^{-1}, \quad (2.8)$$

$$\frac{dB}{dr} = 2B(r) \frac{d\Phi}{dr}, \quad (2.9)$$

where  $M(r)$  is related to the metric factor  $A(r)$  through

$$A(r) = \left[ 1 - \frac{GM(r)}{c^2 r} \right]^{-1}, \quad (2.10)$$

and is interpreted as the mass contained within a radius  $r$ . It obeys the mass equation

$$\frac{dM}{dr} = 4\pi r^2 \rho(r), \quad M(0) = 0, \quad (2.11)$$

that arises from the  $\mu = \nu = 0$  component of the Einstein field equations. These equations are the general relativistic versions of the hydrostatic equilibrium equations of regular stellar structure, with Eq. 2.7 reducing to the familiar

$$\frac{dP}{dr} = -\frac{GM(r)}{r^2} \rho(r), \quad (2.12)$$

in the Newtonian limit,  $GM(r)/c^2 r \ll 1$ .

The radius of the star,  $R_*$ , is identified as the point at which the pressure and density vanish,  $P(R_*) = \rho(R_*) = 0$ . In the region outside the star,  $r > R_*$ , the total mass remains constant at the total mass of the star,  $M(r \geq R_*) = M_*$ , and so the only non-trivial structure functions are the metric factors. Solving Eq. 2.9 with  $P(r) = 0$  and constant  $M(r)$  for  $B(r)$  becomes elementary while the result for  $A(r)$  is trivial, leaving us with

$$A(r) = \left[ 1 - \frac{GM_*}{c^2 r} \right]^{-1}, \quad B(r) = 1 - \frac{GM_*}{c^2 r}, \quad \text{for } r > R_*, \quad (2.13)$$

and the metric reduces to the familiar Schwarzschild metric outside the star. Continuity of the metric at  $r = R_*$  enforces a second boundary condition for  $B(r)$ ,

$$B(R_*) = 1 - \frac{GM_*}{c^2 R_*}. \quad (2.14)$$

The final boundary condition required is the central pressure  $P(0) = P_c$ , or equivalently the central density/baryon number density. This is the only free parameter in the system and hence, for a given EoS, uniquely determines the stellar structure. All stars generated by an EoS can therefore be represented as a one-parameter sequence, typically represented as the mass-radius relation for the model.

Given all the above, we can write a simple recipe for constructing a model of a compact object:

1. Select an EoS to describe the constituent matter.

2. Specify the central pressure of the star,  $P_c$ .
3. Integrate the coupled system of differential equations 2.7, 2.8, 2.11 from the centre of the star outward until the pressure vanishes.
4. Use the boundary condition Eq. 2.14 to normalise the metric function  $B(r)$ .

In general, additional quantities will be present in the EoS, such as chemical potentials or the speed of sound, that may be subject to additional constraints. These quantities will need to be calculated at each step of the integration alongside the other EoS quantities.

## 2.2 White Dwarfs

The fate of main sequence stars of mass below  $M_\star \lesssim 8M_\odot$  is to end their life cycles as a white dwarf. Consequently, these compact stellar remnants, which are supported against gravitational collapse by electron degeneracy pressure, are the most abundant stars in the Galaxy ( $\gtrsim 90\%$ ). They are born at very high temperatures and cool down over billions of years. Observations of the coldest WDs therefore contain information on the star formation history of the Galaxy.

The vast majority of observed WDs are composed primarily of carbon and oxygen, plus small traces of elements heavier than helium. At the extremely high densities found in WDs  $\sim 10^6 - 10^{10} \text{ g cm}^{-3}$ , electrons are strongly degenerate and determine the WD equation of state (EoS) and internal structure. The stellar core resembles a Coulomb lattice of ions surrounded by degenerate electrons, which implies that the WD core is isothermal and a very good thermal conductor. The degenerate core is enclosed by a thin envelope that accounts for  $\lesssim 1\%$  of the total mass [137].

The outer layers form an atmosphere that is rich in lighter elements such as hydrogen or helium, where the exact composition depends on the evolution of the WD progenitor and changes as the WD cools. This atmosphere is non-degenerate and extremely opaque to radiation, with an EoS that is subject to finite temperature effects.

### 2.2.1 The FMT Equation of State

In the limit of zero temperature, the simplest way to obtain the WD EoS is to assume an ideal Fermi gas of degenerate electrons, for a WD that is primarily composed of a single element. Corrections to the non-interacting electron picture were introduced early by Salpeter [138]. By introducing the Wigner-Seitz (WS) cell

approximation and assuming point-like nuclei, Salpeter obtained an analytical EoS that accounts for interactions between electrons and ions as well as other Coulomb corrections. These corrections, in general, depend on the chemical composition of the star.

More recently, it has been shown that the treatment of matter at high pressures presented by Feynman, Metropolis and Teller [139] can be extended to consistently take into account weak interactions and relativistic effects [140, 141], and incorporates Coulomb corrections in a more natural manner than the Salpeter EoS. The resulting Feynman-Metropolis-Teller (FMT) EoS is obtained by considering a relativistic Thomas-Fermi model within Wigner-Seitz cells of radius  $R_{\text{WS}}$ . For degenerate, relativistic, electrons, the equilibrium condition is that the Fermi energy,  $E_e^F$ , is constant within the cell,

$$E_e^F = \sqrt{(p_e^F)^2 + m_e^2} - m_e - eV(r) = \text{constant}, \quad (2.15)$$

where  $V(r)$  is the Coulomb potential inside the cell,  $p_e^F$  is the electron Fermi momentum,  $m_e$  is the electron mass and  $e$  is the electric charge. To obtain an integrable solution for the energy density near the origin, it is necessary to introduce a finite size for the nucleus, with radius  $R_c = \Delta\lambda_\pi Z^{1/3}$ , where  $\lambda_\pi$  is the pion Compton wavelength,  $\Delta \approx (r_0/\lambda_\pi)(A/Z)^{1/3}$ ,  $Z$  is the proton number,  $A$  is the atomic mass, and  $r_0$  is an empirical constant  $\sim 1.2$  fm. The proton and electron number densities inside the cell are then given by

$$n_p = \frac{(p_p^F)^3}{3\pi^2} = \frac{3Z}{4\pi R_c^3} \theta(R_c - r) = \frac{3}{4\pi} \left( \frac{1}{\Delta\lambda_\pi} \right)^3 \theta(R_c - r), \quad (2.16)$$

$$n_e = \frac{(p_e^F)^3}{3\pi^2} = \frac{1}{3\pi^2} \left[ \hat{V}^2(r) + 2m_e \hat{V}(r) \right]^{3/2}, \quad (2.17)$$

$$\hat{V}(r) = eV(r) + E_e^F. \quad (2.18)$$

The Coulomb potential satisfies the Poisson equation

$$\nabla^2 V(r) = -4\pi e[n_p(r) - n_e(r)], \quad (2.19)$$

with requiring global charge neutrality of the cell enforcing the boundary conditions

$$\left. \frac{dV}{dr} \right|_{r=R_{\text{WS}}} = V(R_{\text{WS}}) = 0. \quad (2.20)$$

In practice, it is beneficial to work with dimensionless quantities, and so we define  $x = r/\lambda_\pi$  and  $\chi(r) = r\hat{V}(r)$ , such that  $x_c = R_c/\lambda_\pi$  and  $x_{\text{WS}} = R_{\text{WS}}/\lambda_\pi$ . Using these expressions results in the relativistic Thomas-Fermi equation

$$\frac{1}{3x} \frac{d^2 \chi}{dx^2} = -\frac{\alpha_{\text{EM}}}{\Delta^3} \theta(x_c - x) + \frac{4\alpha_{\text{EM}}}{9\pi} \left[ \frac{\chi^2(x)}{x^2} + 2 \frac{m_e}{m_\pi} \frac{\chi(x)}{x} \right]^{3/2}, \quad (2.21)$$

with the boundary conditions

$$\chi(0) = 0, \quad \left. \frac{d\chi}{dx} \right|_{x_{\text{WS}}} = \frac{\chi(x_{\text{WS}})}{x_{\text{WS}}}. \quad (2.22)$$

By solving these equations, we can obtain the relevant thermodynamic quantities, namely the electron and proton number densities, electron chemical potential, and the energy and pressure of the cell. The electron chemical potential is obtained by evaluating Eq. 2.15 at the cell radius, noting that the Coulomb potential must vanish there, which results in the usual expression<sup>2</sup>

$$\varepsilon_{F,e} = \sqrt{(p_e^F)^2 + m_e^2} - m_e. \quad (2.23)$$

The energy and pressure of the cell can then be obtained following the analysis presented in ref. [141]. The cell energy gains contributions from the nuclear mass, electron kinetic energy, and Coulomb interactions, such that

$$E_{\text{tot}} = M_N + E_k + E_C, \quad (2.24)$$

$$E_k = \int_0^{R_{\text{WS}}} 4\pi r^2 [\mathcal{E}_e(r) - m_e n_e(r)] dr, \quad (2.25)$$

$$E_C = \frac{1}{2} \int_{R_c}^{R_{\text{WS}}} 4\pi r^2 e[n_p(r) - n_e(r)] V(r) dr, \quad (2.26)$$

where

$$\mathcal{E}_e(r) = \frac{1}{\pi^2} \int_0^{p_e^F} p^2 \sqrt{p^2 + m_e^2} dp, \quad (2.27)$$

is the electron energy density, and  $M_N$  is the mass of the nucleus. The energy density of the cell is then simply

$$\rho_{\text{WS}} = \frac{E_{\text{tot}}}{V_{\text{WS}}}, \quad (2.28)$$

where  $V_{\text{WS}} = 4\pi R_{\text{WS}}/3$  is the volume of the WS cell. The only contribution to the internal cell pressure comes from the electrons,

$$P_e(r) = \frac{1}{3\pi^2} \int_0^{p_e^F} \frac{p^4}{\sqrt{p^2 + m_e^2}} dp, \quad (2.29)$$

with the total pressure of the cell being  $P_{\text{tot}} = P_e(R_{\text{WS}})$ . Finally, the EoS is then obtained by solving Eq. 2.21 for various cell radii, yielding a relation between  $E_{\text{tot}}$  and  $P_{\text{tot}}$  parameterised by the radius of the Wigner-Seitz cell.

---

<sup>2</sup>We use the symbol  $\varepsilon_{F,i}$  to represent the chemical potential minus the mass of a particle species  $i$ , reserving  $\mu_{F,i}$  for the full chemical potential.

EoS	WD <sub>1</sub>	WD <sub>2</sub>	WD <sub>3</sub>	WD <sub>4</sub>
$\rho_c$ [g cm <sup>-3</sup> ]	$1.47 \times 10^6$	$3.84 \times 10^7$	$3.13 \times 10^8$	$2.31 \times 10^{10}$
$M_\star$ [ $M_\odot$ ]	0.440	1.000	1.252	1.384
$R_\star$ [km]	$9.39 \times 10^3$	$5.38 \times 10^3$	$3.29 \times 10^3$	$1.25 \times 10^3$
$v_{\text{esc}}(R_\star)$ [km/s]	$3.72 \times 10^3$	$7.03 \times 10^3$	$1.01 \times 10^4$	$1.71 \times 10^4$

**Table 2.1:** Four configurations for white dwarfs composed of carbon, with an FMT EoS. Shown are the central densities,  $\rho_c$ , stellar mass  $M_\star$  and radius  $R_\star$ , and escape velocity at the edge of the WD,  $v_{\text{esc}}$ .

Different WD configurations can be obtained, assuming a non-rotating spherically symmetric star, by solving the Tolman-Oppenheimer-Volkoff (TOV) equations [135, 136] coupled to the FMT EoS with different initial conditions for the pressure at the centre of the star. In Fig. 2.1 we show radial profiles for  $n_e$  (top left),  $\mu_{F,e}$  (top right), and escape velocity  $v_{\text{esc}}$  (bottom) for the carbon WDs in Table 2.1. Note that the difference in radius between the lightest and heaviest WD in Table 2.1 spans almost one order of magnitude, while the electron number densities in the core can vary up to 4 orders of magnitude (see top left panel). As expected, electrons are more degenerate in more compact WDs and become relativistic (see top right panel). The escape velocity can reach  $\mathcal{O}(0.1 c)$  at the interior of the most compact WDs, while for very low mass WDs it can be as low as  $\sim 0.003 c$ .

The mass-radius relations obtained from a zero-temperature EoS begin to deviate from observations for low-mass WDs. To address this discrepancy, finite temperature effects can be introduced to the EoS [142]. The extension to finite temperatures is made by reintroducing the temperature dependence in the Fermi-Dirac distributions. Now, the electron chemical potential is no longer simply the Fermi energy of the system due to thermal corrections. Define the finite temperature Fermi-Dirac integrals of degree  $s$  as

$$F_s(\eta, \beta) = \int_0^\infty \frac{t^s \sqrt{1 + (\beta/2)t}}{1 + e^{t-\eta}} dt, \quad (2.30)$$

where we define the dimensionless quantities

$$t = \frac{E_e - m_e c^2}{k_B T_\star}, \quad (2.31)$$

$$\eta = \frac{\varepsilon_{F,e}}{k_B T_\star}, \quad (2.32)$$

$$\beta = \frac{k_B T_\star}{m_e c^2}, \quad (2.33)$$

for a star at temperature  $T_\star$ . The Thomas-Fermi equilibrium condition within the

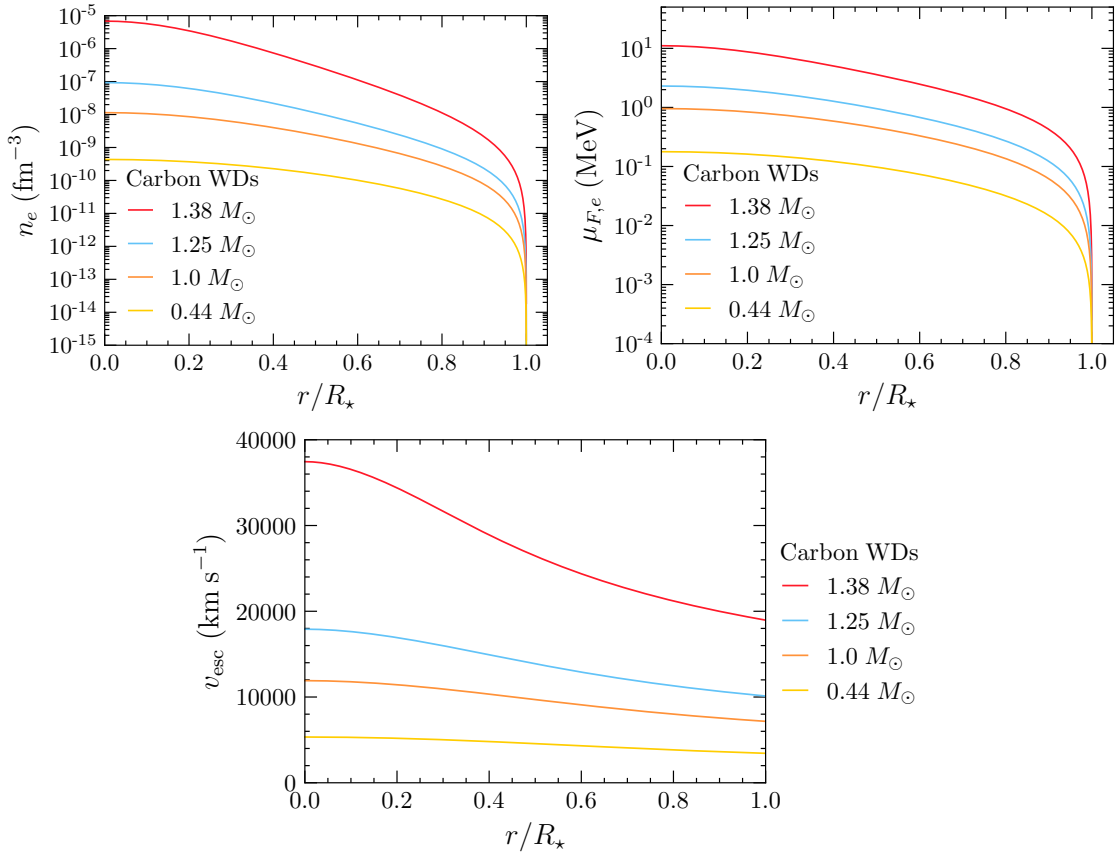


**Figure 2.1:** Electron number density (top left), chemical potential (top right), and escape velocity (bottom) radial profiles for the carbon WDs with FMT EoS in Table 2.1. The radial distance of each profile has been normalised to the radius of the star.

WS cell is now given by

$$\varepsilon_{F,e}(r) - eV(r) = k_B T_\star \eta(r) - eV(r) = \text{constant}, \quad (2.34)$$

with the Coulpmb potential vanishing at the boundary of the cell as before. We now make the change of variables into the dimensionless quantities  $\chi/r = \varepsilon_{F,e}/(\hbar c)$  and  $x = x/x_{\text{WS}}$  so that the Poisson equation 2.19 becomes

$$\frac{d^2\chi}{dx^2} = -4\pi\alpha_{\text{EM}}x \left( \frac{3}{4\pi\Delta^3} \theta(x_c - x) - \frac{\sqrt{2}}{\pi^2} \left( \frac{m_e}{m_\pi} \right)^2 [F_{1/2}(\eta, \beta) + \beta F_{3/2}(\eta, \beta)] \right), \quad (2.35)$$

$$\eta(x) = \left( \frac{1}{\lambda_\pi T_\star} \right) \frac{\chi(x)}{x}, \quad (2.36)$$

with the same boundary conditions as in Eq. 2.22.

The total energy of the cell remains very similar to the zero-temperature case, the main differences being it gains a contribution from the thermal motion of the nucleus,

$$E_{\text{th}} = \frac{3}{2} k_B T_*, \quad (2.37)$$

and that the electron energy density is now given by

$$\mathcal{E}_e = m_e n_e + \frac{\sqrt{2}}{\pi^2} m_e^4 \beta^{5/2} [F_{3/2}(\eta, \beta) + \beta F_{5/2}(\eta, \beta)]. \quad (2.38)$$

The pressure of the cell will now gain contributions from the motion of the nucleus as well as the electron, such that the total pressure is

$$P_{\text{tot}} = P_N + P_e, \quad (2.39)$$

$$P_N = \frac{2}{3} \frac{E_{\text{th}}}{V_{\text{ws}}} = \frac{T_*}{V_{\text{ws}}}, \quad (2.40)$$

$$P_e = \frac{2^{3/2}}{3\pi} m e^4 \beta^{5/2} [F_{3/2}(\eta(x_{\text{ws}}), \beta) + \beta F_{5/2}(\eta(x_{\text{ws}}), \beta)]. \quad (2.41)$$

In Fig. 2.2 we show the Mass-Radius relations obtained from the zero temperature FMT EoS together with several finite temperature configurations. As can be seen, the deviations from the zero temperature approximation begin at rather high temperatures,  $T_* \gtrsim 10^7$  K, for masses  $\lesssim 0.6 M_\odot$ . Additionally, we show observations of WDs from the Gaia early data release 2 (EDR2) report [143] as the blue dots. As mentioned above, the Mass-Radius relation seen from these observations significantly deviates from the zero temperature EoS as low masses. Note that while not represented in this figure, the temperature of the WDs increases in a similar gradient as would be expected from the FMT EoS.

Given the non-linear nature of the differential equations that describe the FMT EoS (both at zero and finite temperatures), solving the system is a numerically challenging task. As there are no publically available resources to help solve these systems, a significant amount of time was put into solving this problem. As such, we have outlined in Appendix **ADD THIS APPENDIX** the method employed in numerically solving the differential equations.

### 2.2.2 Observational Status

## 2.3 Neutron Stars

[Add some intro remarks](#)

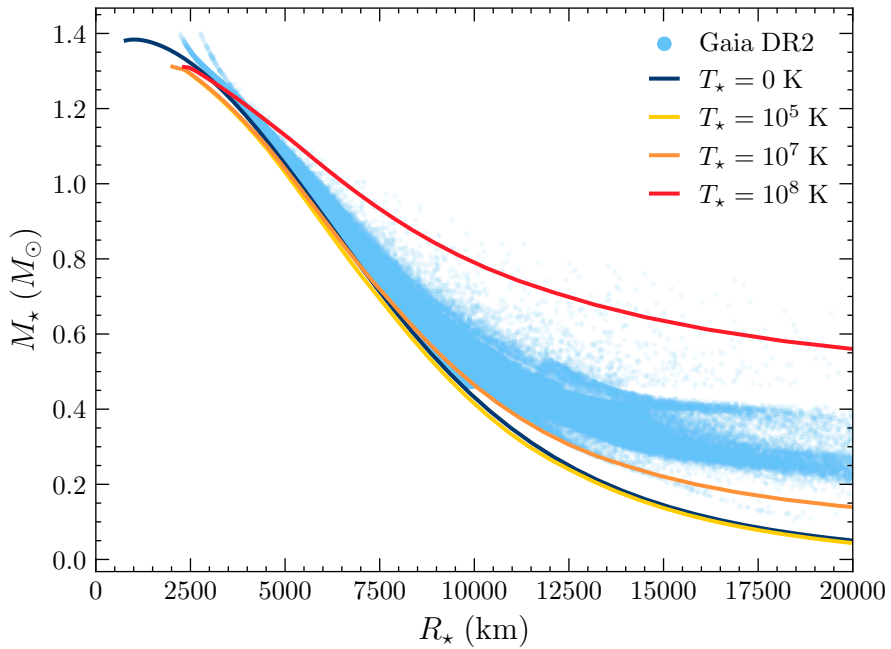


**Figure 2.2:** Mass-Radius relation of WDs calculated from the FMT EoS in the zero temperature approximation (dark blue), at  $10^5$  K (yellow),  $10^7$  K (orange), and  $10^8$  K (red), together with observed WDs from Gaia EDR2 observations [143] (light blue dots).

The internal structure of an NS is significantly more complicated than that of a WD. Broadly speaking, an NS can be divided into five main regions. Working from the outside in, these are:

### Atmosphere

The atmosphere is an extremely thin layer of plasma that makes up less than 1% of the NS mass. However, it plays an extremely important role as the observed spectrum radiation emitted by the star must pass through this star. This radiation contains valuable information about various properties of the star.

### Outer Crust

The outer crust is the thin layer of ionized Iron-56 nuclei that extends down until the density reaches the neutron drip point,  $\rho_* = \rho_{\text{ND}} \sim 4.3 \times 10^{11} \text{ g cm}^{-3}$ . This is the density at which neutrons begin to drip from the nuclei as their chemical potentials

approach zero. The ionized electrons form a non-relativistic but degenerate gas, with their chemical potentials increasing as the density increases. This leads to the “neutronisation” of the nuclei as the beta-capture of electrons by protons increases.

### Inner Crust

The density within the inner crust spans the range between  $\rho_{\text{ND}} \lesssim \rho_* \lesssim 0.5\rho_0$ , with  $\rho_0 \sim 2.8 \times 10^{14} \text{ g cm}^{-3}$  the nuclear saturation density (i.e. the density of nuclear matter). Here, the neutrons that have dripped from the nuclei will potentially form a superfluid. Towards the crust-core boundary, the nuclear lattice begins taking on interesting topological structures that are distinguished by the configuration of the voids in the lattice. These are known as the so-called *pasta phases* of nuclear matter:

- 2D void cylinders creating spaghetti structures of nuclei
- Planar voids with slabs of nuclei forming lasagna sheets
- 3D cylindrical voids leading to thin 2D cylinders of nuclear ziti
- 3D spherical voids enclosed by ravioli
- 2D circular voids in sheets of Swiss cheese

Eventually, the nuclear matter becomes a uniform medium<sup>3</sup>.

### Outer Core

Once densities go above  $0.5\rho_0$ , the nuclear clusters will dissolve into a homogenous fluid that is composed of neutrons, protons, electrons, and muons known as *npeu* matter. The relative abundances of the species,  $Y_i = n_i/n_b$ , are dictated by the conditions of electrical neutrality and beta-equilibrium. Charge neutrality dictates that the abundances of the charged particles obeys

$$Y_p = Y_e + Y_\mu, \tag{2.42}$$

while beta-equilibrium refers to the balance between the weak decays of neutrons and the electron/muon capture by the protons,




---

<sup>3</sup>The nuclear marinara sauce, if you will

with  $\ell = e, \mu$ . Muons will begin to replace electrons in these reactions once the electron chemical potential exceeds the mass of the muon,  $\mu_{F,e} \gtrsim m_\mu = 105.7 \text{ MeV}$ . As the species are all degenerate, muons cannot decay into electrons, imposing the constraint

$$\mu_{F,e} = \mu_{F,\mu}, \quad (2.45)$$

on the chemical potentials. The outer core region ends once the density reaches  $\rho_\star \sim 2\rho_0$ , and we transition into the inner core.

### Inner Core

The densities within the inner cores of NSs extend between  $2\rho_0 \lesssim \rho_\star \lesssim (10 - 15)\rho_0$  and are hence a mystery to this day. As the density exceeds well above any material that can be produced in a laboratory, the exact composition of this region is unknown and depends on the equation of state one adopts to describe it. Some of the more well-known candidates are

- The appearance of hyperonic matter, i.e. nucleons containing a valence strange quark. These being to appear once the neutron chemical potential equals the  $\Lambda^0$  hyperon, with the  $\Xi^-$  appearing once its chemical potential equals the sum of the chemical potentials of the neutrons and electrons.
- Pion/Kaon condensates. These are Bose-Einstein condensates of pion/kaon-like excitations, with the kaon also containing a valence strange quark.
- A quark-gluon plasma comprised of deconfined quarks ( $u, d$  and  $s$ ) and gluons.

Unlike the WDs discussed above, there are far fewer observations of NSs that allow us to constrain the various EoS models. However, the onset of gravitational wave astronomy has begun to see more and more constraints being placed on these models. **talk about the largest NS mass and the grav wave observations that constrain the EoS**

#### 2.3.1 Observational Status



# 3

## Capture Part 1: Point Like Targets

*Review capture in the Sun, move to what's needed for COs in general, then specify to WDs (ions + electrons) and NS (interacting baryons)*

One of the most essential quantities we will be interested in is the rate at which dark matter is captured with the star. In this chapter, we focus on building up the formalism of dark matter capture within compact objects, outlining how this differs from the standard calculation for capture in the Sun. We restrict our analysis to scattering off of point-like targets relevant for leptonic species, i.e. electrons in White Dwarfs and electrons and muons in Neutron Stars. The complications that arise due to the finite size of hadronic targets will be discussed in the next chapter.

### 3.1 Dark Matter Capture in the Sun

Before jumping into the capture formalism relevant to compact objects, it will serve us well to review the formalism laid out by Gould for capture in the Sun [93, 94].

To begin, we consider the flux of dark matter particles that pass through a spherical shell a large distance  $R$  from the star, where the gravitational field is negligible. For this, we need to know the distribution function of the relative velocity between the DM and the stellar constituents. The velocity distribution function will be spatially isotropic, and so for simplicity we will assume that the

DM follows a Maxwell-Boltzmann distribution function,

$$f_\infty(\tilde{u}_\chi)d\tilde{u}_\chi = 4\pi \left(\frac{3}{2\pi}\right)^{3/2} \frac{\tilde{u}_\chi^2}{v_d^2} \exp\left(-\frac{3\tilde{u}_\chi^2}{2v_d^3}\right) d\tilde{u}_\chi, \quad (3.1)$$

where  $\tilde{u}_\chi$  is the DM velocity in the halo, and  $v_d$  is the DM halo velocity dispersion.

Taking into account the motion of the star through the halo and the thermal motion of the constituents, which are assumed to follow a Maxwell-Boltzmann distribution, gives the relative velocity between the DM and targets,  $u_\chi$ . The distribution function for the relative velocity can be expressed as [95]

$$f_{\text{MB}}(u_\chi)du_\chi = \frac{u_\chi}{v_\star} \sqrt{\frac{3}{2\pi(v_d^2 + 3T_\star/m_T)}} \left( e^{-\frac{3(u_\chi - v_\star)^2}{2(v_d^2 + 3T_\star/m_T)}} - e^{-\frac{3(u_\chi + v_\star)^2}{2(v_d^2 + 3T_\star/m_T)}} \right), \quad (3.2)$$

where  $v_\star$  is the star's velocity in the halo rest frame<sup>1</sup>,  $T_\star$  is the temperature of the star, and  $m_T$  is the mass of the target.

Returning to the large spherical shell of radius  $R$ , given the velocity distribution function, we can obtain the flux of DM through this surface. The rate of DM particles passing through a surface element  $d\tilde{A}$  with velocity between  $u_\chi$  and  $u_\chi + du_\chi$ , with an angle to the normal of  $d\tilde{A}$  between  $\tilde{\theta}$  and  $\tilde{\theta} + d\tilde{\theta}$  and an azimuthal angle between  $\tilde{\phi}$  and  $\tilde{\phi} + d\tilde{\phi}$  is given by [92]

$$\frac{dN_\chi}{dt} = \frac{\rho_\chi}{m_\chi} f_{\text{MB}}(u_\chi) \vec{u} \cdot d\vec{A} du_\chi \frac{d\tilde{\Omega}}{4\pi} \quad (3.3)$$

$$= \frac{\rho_\chi}{m_\chi} f_{\text{MB}}(u_\chi) u_\chi \cos \tilde{\theta} d\tilde{A} du_\chi \frac{d \cos \tilde{\theta} d\tilde{\phi}}{4\pi} \quad (3.4)$$

$$= \frac{1}{4} \frac{\rho_\chi}{m_\chi} f_{\text{MB}}(u_\chi) u_\chi d\tilde{A} du_\chi d \cos^2 \tilde{\theta}, \quad (3.5)$$

where we have integrated over the azimuthal angle  $\tilde{\phi}$  due to the isotropy of the system. The number density of the DM is included through the  $\rho_\chi/m_\chi$  factor. Integrating over the area of the sphere is trivial due to isotropy, leaving us with

$$\frac{dN_\chi}{dt} = \pi \frac{\rho_\chi}{m_\chi} f(u_\chi) u_\chi du_\chi d \cos^2 \tilde{\theta}, \quad (3.6)$$

with the integration interval for  $\cos^2 \tilde{\theta}$  being  $(0, 1)$ .

As the DM begins to infall from this large distance  $R$  to a closer distance  $r$ , the star's gravitational field will boost the velocity by the local escape velocity  $v_e(r)$

---

<sup>1</sup>This is the frame where the DM has an average velocity of zero.

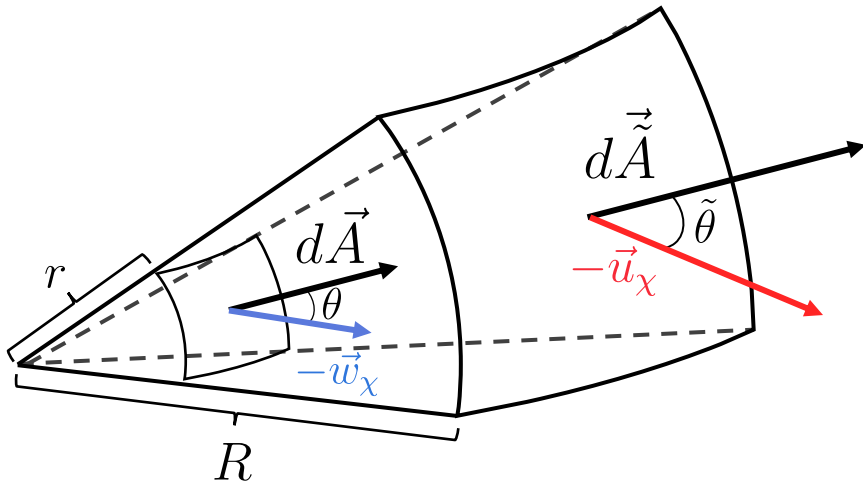


**Figure 3.1:** Geometry of the capture process. The azimuthal angles are not shown for simplicity as they can be integrated over trivially.

such that

$$w_\chi^2(r) = u_\chi^2 + v_e^2(r), \quad (3.7)$$

$$v_e^2(r) = \frac{2GM_\star}{R_\star} + \int_r^{R_\star} \frac{GM_\star(r')}{r'^2} dr'. \quad (3.8)$$

Due to the conservation of angular momentum, we can relate the angular momentum of the DM at the two distances  $R$  and  $r$  such that

$$J_\chi = m_\chi Ru_\chi \sin \tilde{\theta} = m_\chi rw_\chi(r) \sin \theta \leq m_\chi rw_\chi(r) \equiv J_{\max}, \quad (3.9)$$

where  $\theta$  is the incident angle of the DM at the closer distance  $r$ , and we have defined the maximum angular momentum  $J_{\max}$  corresponding to a linear DM trajectory.

Changing integration variables from  $\cos^2 \tilde{\theta}$  to  $J_\chi$  allows us to write the number of DM particles passing through the shell per unit volume as

$$\frac{dN_\chi}{dt} = 2\pi \frac{\rho_\chi}{m_\chi} \frac{f_{\text{MB}}(u_\chi)}{u_\chi} r^2 w_\chi^2(r) \frac{J_\chi dJ_\chi}{J_{\max}^2} du_\chi. \quad (3.10)$$

The geometry of the system is shown in Fig. 3.1 for clarity.

The probability that the DM interacts with the constituents of the shell depends on the interaction rate,  $\Omega(w_\chi)$ , multiplied by the time spent in the shell,  $dt = dr/\dot{r}$ .

Hence, the probability of scattering within the shell is

$$\Omega(w_\chi) \frac{dr}{\dot{r}} = 2\Omega(w_\chi) \frac{1}{w_\chi} \left( 1 - \left( \frac{J_\chi}{rw_\chi} \right)^2 \right)^{-1/2} \Theta(J_{\max} - J_\chi) dr, \quad (3.11)$$

where the factor of 2 is due to the DM having two opportunities to pass through the shell, once when incoming and another after turning around<sup>2</sup>. The step-function is put in to ensure the angular momentum does not exceed its maximum allowed value.

For a scattered DM to be considered captured, it must lose enough energy in the collision to become gravitationally bound. The rate at which a DM particle scatters from an initial velocity  $w_\chi$  to a final velocity  $v < v_e(r)$  is given by [93–95]

$$\Omega^-(w_\chi) = \int_0^{v_e} R^-(w_\chi \rightarrow v) dv, \quad (3.12)$$

$$R^-(w_\chi \rightarrow v) = \int n_T(r) \frac{d\sigma_{\chi T}}{dv} |\vec{w}_\chi - \vec{u}_T| f_T(u_T) d^3 \vec{u}_T, \quad (3.13)$$

with  $R^-(w_\chi \rightarrow v)$  being the differential interaction rate,  $n_T$  is the target number density,  $u_T$  is the target velocity and  $f_T(u_T)$  is the corresponding distribution function, and  $d\sigma_{\chi T}/dv$  is the differential cross-section. The minus superscript is used to signify that this is the down scattering rate, i.e. the rate of interactions leading to the DM losing energy.

Finally, we obtain the capture rate by multiplying Eqs. 3.10 and 3.11 and integrate over the angular momentum to give the result

$$C = \int_0^{R_*} dr 4\pi r^2 \int_0^\infty du_\chi \frac{\rho_\chi}{m_\chi} \frac{f_{\text{MB}}(u_\chi)}{u_\chi} w_\chi(r) \Omega^-(w_\chi). \quad (3.14)$$

This result is rather generic, as the choice of DM model will only dictate the form of the differential cross section in Eq. 3.13. In fact, as written above, the distribution function for the relative velocity far from the star can be any isotropic distribution function. The MB form was chosen as it allows for a simple analytic form.

## 3.2 Capture in Compact Objects

Having reviewed the capture process in non-relativistic stars, we can begin discussing the necessary modifications required when considering relativistic stars. In this section, we consider the two major modifications that need to be made:

---

<sup>2</sup>The radial velocity  $\dot{r}$  is a standard result in orbital mechanics and can be obtained from the central force Lagrangian.

- The corrections from General Relativity due to the extreme gravitational fields. This ultimately alters the flux of DM passing through the star, boosting it through gravitational focusing.
- Accounting for the relativistic and degenerate nature of the star's constituents in the interaction rate.

The former is generic to neutron stars and white dwarfs, while the latter is required for all NS constituents, but only the electrons in a WD are degenerate and relativistic. The ions of the WD are non-relativistic and non-degenerate and, hence, can be treated the same as the Sun's constituents.

### 3.2.1 General Relativistic Corrections to the Capture Rate

Far from the star, the physics is the same as in the previous section. The deviations arise as the DM falls into the gravitational potential of the star. We begin by following the DM along its trajectory, moving from a distance  $R \gg R_\star$  to a closer distance  $r$ . Hence, we are working in the DM rest frame and calculating the rate at which the DM passes through the shell *per unit of proper time*,  $\tau$ . The proper time interval is related to the metric through

$$d\tau^2 = B(r)dt^2 - A(r)dr^2 - r^2d\Omega^2, \quad (3.15)$$

with  $B(r)$  and  $A(r)$  defined in Chapter 2.

Following the same arguments as in the non-relativistic case, the flux of DM passing through the shell is

$$\frac{dN_\chi}{d\tau} = 2\pi \frac{\rho_\chi}{m_\chi} \frac{f_{\text{MB}}(u_\chi)}{u_\chi} du_\chi \frac{J_\chi dJ_\chi}{m_\chi^2}, \quad (3.16)$$

which takes the same form as Eq. 3.10, with the physical difference being that this is the rate with respect to the proper time.

The probability that DM scatters within the shell and is captured is  $2\hat{\Omega}^-(r)d\tau$ , where  $\hat{\Omega}^-(r)$  is the interaction rate with respect to the proper time, and  $d\tau$  is the proper time taken to move from coordinate  $r$  to  $r + dr$ . The factor of 2 once again accounts for the DM crossing the shell twice per orbit. For calculation purposes, we need to relate this to the interaction rate seen by a distant observer,  $\Omega^-(r)$ , that is done through

$$\hat{\Omega}^-(r)d\tau = \frac{1}{\sqrt{g_{tt}}} \Omega^-(r)d\tau = \frac{1}{\sqrt{B(r)}} \Omega^-(r)d\tau. \quad (3.17)$$

Now, the proper time that the DM spends inside a shell of thickness  $dr$  will be<sup>3</sup>

$$d\tau = \left( \frac{d\tau}{dt} \right) dt = B(r) \frac{dr}{\dot{r}} = \frac{\sqrt{B(r)} dr}{\sqrt{\frac{1}{A(r)} \left[ 1 - B(r) \left( 1 + \frac{J_\chi^2}{m_\chi^2 r^2} \right) \right]}}. \quad (3.18)$$

Combining everything together gives us the differential capture rate,

$$dC = 2\pi \frac{\rho_\chi}{m_\chi} \frac{f_{\text{MB}}(u_\chi)}{u_\chi} du_\chi \frac{dJ_\chi^2}{m_\chi^2} \frac{\Omega^-(r) \sqrt{A(r)} dr}{\sqrt{1 - B(r) \left( 1 + \frac{J_\chi^2}{m_\chi^2 r^2} \right)}}. \quad (3.19)$$

As the total number of targets in the star,  $N_T$ , needs to satisfy

$$N_T = \int_0^{R_*} 4\pi r^2 n_T(r) \sqrt{A(r)} dr, \quad (3.20)$$

where  $n_T(r)$  is the number density that appears in the interaction rate, we absorb the factor  $\sqrt{A(r)}$  into the definition of  $n_T(r)$ , such that  $\Omega^-(r)\sqrt{A(r)} \rightarrow \Omega^-(r)$ . This is due to the number densities obtained by solving the TOV equations already account for the  $\sqrt{A(r)}$  factor.

As before, we have  $w_\chi^2(r) = u_\chi^2 + v_e^2(r)$ , however as the escape velocity will be significantly larger than the ambient DM velocity far from the star, we can safely approximate  $w_\chi^2(r) \approx v_e^2(r)$ . In the relativistic case, the escape velocity can be defined as

$$v_e^2(r) = \left( \frac{dl}{d\tau} \right)^2 = A(r) \left( \frac{dr}{d\tau} \right)^2 + r^2 \left( \frac{d\phi}{d\tau} \right)^2 = 1 - B(r), \quad (3.21)$$

where  $dl$  is a length element. The large boost from the escape velocity also removes the  $u_\chi$  dependence in the kinematics of the interactions and allows us to perform the integration over the initial DM velocity, yielding an overall factor of

$$\int_0^\infty \frac{f_{\text{MB}}(u_\chi)}{u_\chi} du_\chi = \frac{1}{v_\star} \text{Erf} \left( \sqrt{\frac{3}{2}} \frac{v_\star}{v_d} \right). \quad (3.22)$$

To integrate over  $J_\chi^2$ , we need the maximum angular momentum the DM can achieve as it passes through the shell. This can be obtained by requiring the argument of the radical above to remain positive, giving

$$J_{\max} = \sqrt{\frac{1 - B(r)}{B(r)}} m_\chi r. \quad (3.23)$$

---

<sup>3</sup>See Appendix B for the derivation of  $\dot{r} = \frac{dr}{dt}$ .

The factor of  $1/\sqrt{B}$  arises due to the gravitational focusing of the incoming flux of DM [144].

Putting everything together, and integrating over the radius of the star, we are left with the final result for the capture rate of

$$C = \frac{4\pi}{v_\star} \frac{\rho_\chi}{m_\chi} \operatorname{Erf} \left( \sqrt{\frac{3}{2}} \frac{v_\star}{v_d} \right) \int_0^{R_\star} r^2 \frac{\sqrt{1 - B(r)}}{B(r)} \Omega^-(r) dr. \quad (3.24)$$

### 3.2.2 Interaction Rate for Degenerate Targets

## 3.3 White Dwarfs: Electron Targets

## 3.4 Neutron Stars: Leptoinc Targets



# 4

## Capture Rate for Strongly Interacting Baryonic Matter

*The capture formalism developed in the previous chapter is extended to baryonic targets inside neutron stars. Additional complications arise due to their finite size and strong interactions between the baryonic species.*



# 5

## Dark Matter Induced Heating of Neutron Stars

*We analyse the various timescales at play when determining the extent of heating dark matter can induce in neutron stars. This heating occurs in two stages. Kinetic heating requires a significant fraction of the dark matter's kinetic energy to be deposited through scattering. Further annihilation heating requires the captures and annihilation rates to come into equilibrium. The timescales for these processes is calculated and compared to the age of the star.*

### 5.1 Thermalisation Time

### 5.2 Capture-Accretion Equilibrium

### 5.3 Dark Matter Heating

#### 5.3.1 Kinetic Heating

#### 5.3.2 Annihilation Heating



# 6

## Conclusion

*Concluding remarks*



# A

## Kinematics

*Derivation of  $E'_f$  as needed for capture and other kinematics*



# B

## Kinetic Heating

### B.1 DM Orbits in General Isometric Metric

The metric at any point inside or outside the NS can be written as

$$ds^2 = B(r)dt^2 - A(r)dr^2 - r^2(d\theta + \sin\theta d\phi)^2 \quad (\text{B.1})$$

Along an orbit, the conserved conjugate momenta are the angular momentum per unit mass,  $p_\phi = -L$  and the energy per unit mass  $p_t = E_\chi$ , and taking the orbit to lie in the  $\theta = \pi/2$  plane leads to  $p_\theta = 0$ .

The equation which describes the orbit can be obtained from the square of the energy-momentum 4-vector,

$$g_{\alpha\beta}p^\alpha p^\beta - m_\chi^2 = 0 \quad (\text{B.2})$$

$$\implies g^{\alpha\beta}p_\alpha p_\beta - m_\chi^2 = 0 \quad (\text{B.3})$$

with

$$g^{tt} = 1/B(r), \quad g^{rr} = -1/A(r), \quad g^{\phi\phi} = -1/r^2 \quad (\text{B.4})$$

$$\implies 0 = g^{tt}p_t p_t + g^{rr}p_r p_r + g^{\phi\phi}p_\phi p_\phi - m_\chi^2 \quad (\text{B.5})$$

$$= \frac{E_\chi^2}{B(r)} - \frac{1}{A(r)} \left( g_{rr'}p^{r'} \right) \left( g_{rr'}p^{r'} \right) - \frac{L^2}{r^2} - m_\chi^2 \quad (\text{B.6})$$

$$= \frac{E_\chi^2}{B(r)} - m_\chi^2 A(r) \left( \frac{dr}{d\tau} \right)^2 - \frac{L^2}{r^2} - m_\chi^2 \quad (\text{B.7})$$

To find  $dt/d\tau$ , we use

$$p^t = m_\chi \frac{dt}{d\tau} = g^{tt} p_t = \frac{E_\chi}{B(r)} \quad (\text{B.8})$$

$$\implies \frac{dt}{d\tau} = \frac{1}{B(r)} \frac{E_\chi}{m_\chi} \quad (\text{B.9})$$

This gives

$$\left( \frac{dr}{dt} \right)^2 = \frac{B}{\tilde{E}_\chi^2 A} \left[ \tilde{E}_\chi^2 - B(r) \left( 1 + \frac{\tilde{L}^2}{r^2} \right) \right] \quad (\text{B.10})$$

For simplicity, consider orbits that are a straight line ( $\tilde{L} = 0$ ), which has a radial extent  $R$ . This is related to  $\tilde{E}_\chi$  through

$$\tilde{E}_\chi^2 = B(R) \quad (\text{B.11})$$

$$\implies R = \frac{2GM_\star}{1 - \tilde{E}_\chi^2}, \quad R > R_\star \quad (\text{B.12})$$

using  $B(r > R_\star) = 1 - 2GM_\star/r$ .

It is important to note that  $E_\chi$  so far has been the *conserved* energy along the orbit, which for the initial approach is  $E_\chi = m_\chi + \frac{1}{2}m_\chi u^2 \sim m_\chi$ . We now call this energy  $E_\chi^{\text{orbit}}$ , which is related to the DM energy as seen by a distant observer,  $E_\chi^{\text{int}}$ , and is the energy used in calculating the interaction rates, through

$$E_\chi^{\text{orbit}} = \sqrt{g_{tt}} E_\chi^{\text{int}} = \sqrt{B(r)} E_\chi^{\text{int}} \quad (\text{B.13})$$

and as  $E_\chi^{\text{orbit}} < m_\chi$  for all subsequent scatters after capture, eq. B.12 is always positive.

These “orbits” are straight lines that pass through the star’s centre and extend an amount  $R - R_\star$  on either side. Due to the symmetry of the motion, the period of the orbit is then

$$T_{\text{orbit}} = 4 \int_0^R \frac{1}{dr/dt} dr \quad (\text{B.14})$$

More relevant to this application is the time spent inside and outside the star, which is given by

$$T_{\text{inside}} = 4 \int_0^{R_\star} \frac{1}{dr/dt} dr \quad (\text{B.15})$$

$$T_{\text{outside}} = 4 \int_{R_\star}^R \frac{1}{dr/dt} dr \quad (\text{B.16})$$

## B.2 Procedure for calculating kinetic heating time

- Select a point in the star for the DM to scatter off,  $r_{\text{scatter},0}$ .
- DM comes in from infinity with initial energy  $E_\chi \approx m_\chi$
- Boost DM to local energy of  $m_\chi / \sqrt{B(r_{\text{scatter}})}$
- Scatter the DM and calculate initial  $\Delta E_\chi$
- Set local DM energy to  $E_\chi \equiv p^t = m_\chi / \sqrt{B(r_{\text{scatter}})} - \Delta E_\chi$
- Calculate the new conserved energy per unit mass along the orbit as

$$\tilde{E}_\chi^{\text{orbit}} = \sqrt{B(r_{\text{scatter}})} E_\chi / m_\chi = \frac{\sqrt{B(r_{\text{scatter}})}}{m_\chi} (m_\chi / \sqrt{B(r_{\text{scatter},0})} - \Delta E_\chi) \quad (\text{B.17})$$

- Use Equation B.11 to solve for the maximum radius of the orbit,  $R_{\text{orbit}}$ .
- Use equations B.15 and B.16 to calculate  $T_{\text{in}}/(T_{\text{in}} + T_{\text{out}})$
- Adjust the time interval between scatter by  $dt \rightarrow dt(T_{\text{in}}/(T_{\text{in}} + T_{\text{out}}))^{-1}$
- Iterate until  $R_{\text{orbit}} < R_\star$



# Definition of Symbols and Abbreviations

$C_{\text{geo}}$	Geometric Capture Rate	$\mathbf{NS}$	Neutron Star
$\mathbf{DM}$	Dark Matter	$\mathbf{PB}$	Pauli Blocking
$K_\chi$	Dark Matter Kinetic Energy	$\mathbf{QMC}$	Quark-Meson-Coupling EoS
$\rho_\chi$	DM halo density	$\sigma_{\text{th}}$	Threshold Cross Section
$m_\chi$	Dark Matter Mass	$T_{\text{eq}}$	Equilibrium Temperature
$\mathbf{EFT}$	Effective Field Theory	$t_{\text{eq}}$	Capture-Annihilation equilibrium time
$\mathbf{EoS}$	Equation of State	$T_\star$	Temperature of the star
$f_{\text{FD}}$	Fermi-Dirac Distribution	$t_{\text{therm}}$	Thermalisation time
$\epsilon_{F,i}$	Fermi kinetic energy of target species	$v_d$	DM halo dispersion velocity
$ \overline{\mathcal{M}} ^2$	Spin-averaged squared matrix element	$v_\star$	Star velocity
$\mu$	DM-Target mass ratio, $m_\chi/m_i$		



# Bibliography

- [1] Nicole F. Bell et al. “Improved Treatment of Dark Matter Capture in Neutron Stars”. In: *JCAP* 09 (Sept. 15, 2020), p. 028. DOI: [10.1088/1475-7516/2020/09/028](https://doi.org/10.1088/1475-7516/2020/09/028). arXiv: [2004.14888 \[hep-ph\]](https://arxiv.org/abs/2004.14888).
- [2] Nicole F. Bell et al. “Improved Treatment of Dark Matter Capture in Neutron Stars II: Leptonic Targets”. In: *JCAP* 03 (Mar. 26, 2021), p. 086. DOI: [10.1088/1475-7516/2021/03/086](https://doi.org/10.1088/1475-7516/2021/03/086). arXiv: [2010.13257 \[hep-ph\]](https://arxiv.org/abs/2010.13257).
- [3] Nicole F. Bell et al. “Nucleon Structure and Strong Interactions in Dark Matter Capture in Neutron Stars”. In: *Phys. Rev. Lett.* 127.11 (Sept. 10, 2021), p. 111803. DOI: [10.1103/PhysRevLett.127.111803](https://doi.org/10.1103/PhysRevLett.127.111803). arXiv: [2012.08918 \[hep-ph\]](https://arxiv.org/abs/2012.08918).
- [4] Nicole F. Bell et al. “Improved Treatment of Dark Matter Capture in White Dwarfs”. In: *JCAP* 10 (Oct. 29, 2021), p. 083. DOI: [10.1088/1475-7516/2021/10/083](https://doi.org/10.1088/1475-7516/2021/10/083). arXiv: [2104.14367 \[hep-ph\]](https://arxiv.org/abs/2104.14367).
- [5] Filippo Anzuini et al. “Improved Treatment of Dark Matter Capture in Neutron Stars III: Nucleon and Exotic Targets”. In: *JCAP* 11.11 (Nov. 29, 2021), p. 056. DOI: [10.1088/1475-7516/2021/11/056](https://doi.org/10.1088/1475-7516/2021/11/056). arXiv: [2108.02525 \[hep-ph\]](https://arxiv.org/abs/2108.02525).
- [6] Nicole F. Bell et al. “Thermalization and Annihilation of Dark Matter in Neutron Stars”. In: *arXiv:2312.11892 [hep-ph]* (Dec. 2023). arXiv: [2312.11892 \[hep-ph\]](https://arxiv.org/abs/2312.11892).
- [7] F. Zwicky. “On the Masses of Nebulae and of Clusters of Nebulae”. In: *The Astrophysical Journal* 86 (1937), pp. 217–246. DOI: [10.1086/143864](https://doi.org/10.1086/143864).
- [8] Katherine Freese. “Review of Observational Evidence for Dark Matter in the Universe and in Upcoming Searches for Dark Stars”. In: *EAS Publications Series* 36 (May 30, 2009), pp. 113–126. DOI: [10.1051/eas/0936016](https://doi.org/10.1051/eas/0936016). arXiv: [0812.4005 \[astro-ph\]](https://arxiv.org/abs/0812.4005).
- [9] Federico Lelli, Stacy S. McGaugh, and James M. Schombert. “SPARC: Mass Models for 175 Disk Galaxies with Spitzer Photometry and Accurate Rotation Curves”. In: *The Astronomical Journal* 152.6 (2016), p. 157. DOI: [10.3847/0004-6256/152/6/157](https://doi.org/10.3847/0004-6256/152/6/157). arXiv: [1606.09251 \[astro-ph.GA\]](https://arxiv.org/abs/1606.09251).

- [10] Volker Springel, Carlos S. Frenk, and Simon D. M. White. “The Large-Scale Structure of the Universe”. In: *Nature* 440.7088 (2006), p. 1137. DOI: [10.1038/nature04805](https://doi.org/10.1038/nature04805). arXiv: [astro-ph/0604561](https://arxiv.org/abs/astro-ph/0604561).
- [11] Volker Springel et al. “Simulating the Joint Evolution of Quasars, Galaxies and Their Large-Scale Distribution”. In: *Nature* 435.7042 (2005), pp. 629–636. DOI: [10.1038/nature03597](https://doi.org/10.1038/nature03597). arXiv: [astro-ph/0504097](https://arxiv.org/abs/astro-ph/0504097).
- [12] Samuel D. McDermott, Hai-Bo Yu, and Kathryn M. Zurek. “Turning off the Lights: How Dark Is Dark Matter?” In: *Physical Review D* 83.6 (2011), p. 063509. DOI: [10.1103/PhysRevD.83.063509](https://doi.org/10.1103/PhysRevD.83.063509). arXiv: [1011.2907 \[hep-ph\]](https://arxiv.org/abs/1011.2907).
- [13] Sean Tulin and Hai-Bo Yu. “Dark Matter Self-interactions and Small Scale Structure”. In: *Physics Reports* 730 (Feb. 5, 2018), pp. 1–57. DOI: [10.1016/j.physrep.2017.11.004](https://doi.org/10.1016/j.physrep.2017.11.004). arXiv: [1705.02358 \[hep-ph\]](https://arxiv.org/abs/1705.02358).
- [14] David N. Spergel and Paul J. Steinhardt. “Observational Evidence for Self-Interacting Cold Dark Matter”. In: *Physical Review Letters* 84.17 (2000), pp. 3760–3763. DOI: [10.1103/PhysRevLett.84.3760](https://doi.org/10.1103/PhysRevLett.84.3760). arXiv: [astro-ph/9909386](https://arxiv.org/abs/astro-ph/9909386).
- [15] Scott W. Randall et al. “Constraints on the Self-Interaction Cross-Section of Dark Matter from Numerical Simulations of the Merging Galaxy Cluster 1E 0657-5”. In: *The Astrophysical Journal* 679.2 (2008), pp. 1173–1180. DOI: [10.1086/587859](https://doi.org/10.1086/587859). arXiv: [0704.0261 \[astro-ph\]](https://arxiv.org/abs/0704.0261).
- [16] David A. Buote et al. “Chandra Evidence for a Flattened, Triaxial Dark Matter Halo in the Elliptical Galaxy NGC 720”. In: *The Astrophysical Journal* 577.1 (2002), pp. 183–196. DOI: [10.1086/342158](https://doi.org/10.1086/342158). arXiv: [astro-ph/0205469](https://arxiv.org/abs/astro-ph/0205469).
- [17] Jonathan L. Feng. “Dark Matter Candidates from Particle Physics and Methods of Detection”. In: *Ann. Rev. Astron. Astrophys.* 48 (2010), pp. 495–545. DOI: [10.1146/annurev-astro-082708-101659](https://doi.org/10.1146/annurev-astro-082708-101659). arXiv: [1003.0904 \[astro-ph.CO\]](https://arxiv.org/abs/1003.0904).
- [18] Gerard Jungman, Marc Kamionkowski, and Kim Griest. “Supersymmetric Dark Matter”. In: *Phys. Rept.* 267 (1996), pp. 195–373. DOI: [10.1016/0370-1573\(95\)00058-5](https://doi.org/10.1016/0370-1573(95)00058-5). arXiv: [hep-ph/9506380](https://arxiv.org/abs/hep-ph/9506380).
- [19] Gary Steigman, Basudeb Dasgupta, and John F. Beacom. “Precise Relic WIMP Abundance and Its Impact on Searches for Dark Matter Annihilation”. In: *Phys. Rev. D* 86 (2012), p. 023506. DOI: [10.1103/PhysRevD.86.023506](https://doi.org/10.1103/PhysRevD.86.023506). arXiv: [1204.3622 \[hep-ph\]](https://arxiv.org/abs/1204.3622).
- [20] N. Aghanim, Y. Akrami, M. Ashdown, et al. “Planck 2018 Results. VI. Cosmological Parameters”. In: *Astronomy & Astrophysics* 641 (Sept. 1, 2020), A6. DOI: [10.1051/0004-6361/201833910](https://doi.org/10.1051/0004-6361/201833910). arXiv: [1807.06209 \[astro-ph.CO\]](https://arxiv.org/abs/1807.06209).

- [21] Kim Griest and Marc Kamionkowski. “Unitarity Limits on the Mass and Radius of Dark Matter Particles”. In: *Phys. Rev. Lett.* 64 (1990), p. 615. DOI: [10.1103/PhysRevLett.64.615](https://doi.org/10.1103/PhysRevLett.64.615).
- [22] R. D. Peccei and Helen R. Quinn. “CP Conservation in the Presence of Instantons”. In: *Phys. Rev. Lett.* 38 (1977), pp. 1440–1443. DOI: [10.1103/PhysRevLett.38.1440](https://doi.org/10.1103/PhysRevLett.38.1440).
- [23] C. Abel et al. “Measurement of the Permanent Electric Dipole Moment of the Neutron”. In: *Phys. Rev. Lett.* 124.8 (Feb. 29, 2020), p. 081803. DOI: [10.1103/PhysRevLett.124.081803](https://doi.org/10.1103/PhysRevLett.124.081803). arXiv: [2001.11966 \[hep-ex\]](https://arxiv.org/abs/2001.11966).
- [24] Jihn E. Kim. “Weak Interaction Singlet and Strong CP Invariance”. In: *Phys. Rev. Lett.* 43 (1979), p. 103. DOI: [10.1103/PhysRevLett.43.103](https://doi.org/10.1103/PhysRevLett.43.103).
- [25] Mikhail A. Shifman, A. I. Vainshtein, and Valentin I. Zakharov. “Can Confinement Ensure Natural CP Invariance of Strong Interactions?” In: *Nucl. Phys. B* 166 (1980), pp. 493–506. DOI: [10.1016/0550-3213\(80\)90209-6](https://doi.org/10.1016/0550-3213(80)90209-6).
- [26] A. R. Zhitnitsky. “On Possible Suppression of the Axion Hadron Interactions. (In Russian)”. In: *Sov. J. Nucl. Phys.* 31 (1980), p. 260.
- [27] Michael Dine, Willy Fischler, and Mark Srednicki. “A Simple Solution to the Strong CP Problem with a Harmless Axion”. In: *Phys. Lett. B* 104 (1981), pp. 199–202. DOI: [10.1016/0370-2693\(81\)90590-6](https://doi.org/10.1016/0370-2693(81)90590-6).
- [28] Eugenio Del Nobile, Marco Cirelli, and Paolo Panci. “Tools for Model-Independent Bounds in Direct Dark Matter Searches”. In: *Journal of Cosmology and Astroparticle Physics* 10.10 (Oct. 10, 2013), p. 019. DOI: [10.1088/1475-7516/2013/10/019](https://doi.org/10.1088/1475-7516/2013/10/019). arXiv: [1307.5955 \[hep-ph\]](https://arxiv.org/abs/1307.5955).
- [29] A. Liam Fitzpatrick et al. “The Effective Field Theory of Dark Matter Direct Detection”. In: *Journal of Cosmology and Astroparticle Physics* 02.02 (2013), p. 004. DOI: [10.1088/1475-7516/2013/02/004](https://doi.org/10.1088/1475-7516/2013/02/004). arXiv: [1203.3542 \[hep-ph\]](https://arxiv.org/abs/1203.3542).
- [30] Jessica Goodman et al. “Constraints on Dark Matter from Colliders”. In: *Physical Review D* 82.11 (2010), p. 116010. DOI: [10.1103/PhysRevD.82.116010](https://doi.org/10.1103/PhysRevD.82.116010). arXiv: [1008.1783 \[hep-ph\]](https://arxiv.org/abs/1008.1783).
- [31] “Electromagnetic Structure of the Nucleon”. In: *The Structure of the Nucleon*. John Wiley & Sons, Ltd, 2001, pp. 7–51. DOI: [10.1002/352760314X.ch2](https://doi.org/10.1002/352760314X.ch2).
- [32] Giorgio Busoni et al. “On the Validity of the Effective Field Theory for Dark Matter Searches at the LHC”. In: *Phys. Lett. B* 728 (Jan. 20, 2014), pp. 412–421. DOI: [10.1016/j.physletb.2013.11.069](https://doi.org/10.1016/j.physletb.2013.11.069). arXiv: [1307.2253 \[hep-ph\]](https://arxiv.org/abs/1307.2253).

- [33] O. Buchmueller, Matthew J. Dolan, and Christopher McCabe. “Beyond Effective Field Theory for Dark Matter Searches at the LHC”. In: *JHEP* 01 (2014), p. 025. DOI: [10.1007/JHEP01\(2014\)025](https://doi.org/10.1007/JHEP01(2014)025). arXiv: [1308.6799 \[hep-ph\]](https://arxiv.org/abs/1308.6799).
- [34] Giorgio Busoni et al. “On the Validity of the Effective Field Theory for Dark Matter Searches at the LHC Part III: Analysis for the t-Channel”. In: *JCAP* 09 (2014), p. 022. DOI: [10.1088/1475-7516/2014/09/022](https://doi.org/10.1088/1475-7516/2014/09/022). arXiv: [1405.3101 \[hep-ph\]](https://arxiv.org/abs/1405.3101).
- [35] Giorgio Busoni et al. “On the Validity of the Effective Field Theory for Dark Matter Searches at the LHC, Part II: Complete Analysis for the s-Channel”. In: *JCAP* 06 (2014), p. 060. DOI: [10.1088/1475-7516/2014/06/060](https://doi.org/10.1088/1475-7516/2014/06/060). arXiv: [1402.1275 \[hep-ph\]](https://arxiv.org/abs/1402.1275).
- [36] Albert M Sirunyan, Armen Tumasyan, Wolfgang Adam, et al. “Search for Dark Matter Produced with an Energetic Jet or a Hadronically Decaying W or Z Boson at  $\text{Sqrt}(s) = 13 \text{ TeV}$ ”. In: *Journal of High Energy Physics* 07.7 (July 5, 2017), p. 014. DOI: [10.1007/JHEP07\(2017\)014](https://doi.org/10.1007/JHEP07(2017)014). arXiv: [1703.01651 \[hep-ex\]](https://arxiv.org/abs/1703.01651).
- [37] F. Ruppin et al. “Complementarity of Dark Matter Detectors in Light of the Neutrino Background”. In: *Physical Review D* 90.8 (Oct. 7, 2014), p. 083510. DOI: [10.1103/PhysRevD.90.083510](https://doi.org/10.1103/PhysRevD.90.083510). arXiv: [1408.3581 \[hep-ph\]](https://arxiv.org/abs/1408.3581).
- [38] S. J. Asztalos et al. “A SQUID-based Microwave Cavity Search for Dark-Matter Axions”. In: *Phys. Rev. Lett.* 104 (2010), p. 041301. DOI: [10.1103/PhysRevLett.104.041301](https://doi.org/10.1103/PhysRevLett.104.041301). arXiv: [0910.5914 \[astro-ph.CO\]](https://arxiv.org/abs/0910.5914).
- [39] P. Brun, A. Caldwell, L. Chevalier, et al. “A New Experimental Approach to Probe QCD Axion Dark Matter in the Mass Range above  $40\text{\mu eV}$ ”. In: *The European Physical Journal C* 79.3 (Mar. 1, 2019), p. 186. DOI: [10.1140/epjc/s10052-019-6683-x](https://doi.org/10.1140/epjc/s10052-019-6683-x). arXiv: [1901.07401 \[physics.ins-det\]](https://arxiv.org/abs/1901.07401).
- [40] J. Aalbers et al. “First Dark Matter Search Results from the LUX-ZEPLIN (LZ) Experiment”. In: *Physical Review Letters* 131.4 (July 28, 2023), p. 041002. DOI: [10.1103/PhysRevLett.131.041002](https://doi.org/10.1103/PhysRevLett.131.041002). arXiv: [2207.03764 \[hep-ex\]](https://arxiv.org/abs/2207.03764).
- [41] E. Aprile et al. “Search for Coherent Elastic Scattering of Solar  ${}^8\text{B}$  Neutrinos in the XENON1T Dark Matter Experiment”. In: *Phys. Rev. Lett.* 126 (Mar. 1, 2021), p. 091301. DOI: [10.1103/PhysRevLett.126.091301](https://doi.org/10.1103/PhysRevLett.126.091301). arXiv: [2012.02846 \[hep-ex\]](https://arxiv.org/abs/2012.02846).
- [42] Yue Meng et al. “Dark Matter Search Results from the PandaX-4T Commissioning Run”. In: *Phys. Rev. Lett.* 127.26 (Dec. 23, 2021), p. 261802. DOI: [10.1103/PhysRevLett.127.261802](https://doi.org/10.1103/PhysRevLett.127.261802). arXiv: [2107.13438 \[hep-ex\]](https://arxiv.org/abs/2107.13438).

- [43] P. Agnes et al. “Search for Dark-Matter–Nucleon Interactions via Migdal Effect with DarkSide-50”. In: *Phys. Rev. Lett.* 130.10 (Mar. 6, 2023), p. 101001. DOI: [10.1103/PhysRevLett.130.101001](https://doi.org/10.1103/PhysRevLett.130.101001). arXiv: [2207.11967 \[hep-ex\]](https://arxiv.org/abs/2207.11967).
- [44] A.H. Abdelhameed, G. Angloher, P. Bauer, et al. “First Results from the CRESST-III Low-Mass Dark Matter Program”. In: *Physical Review D* 100.10 (Nov. 26, 2019), p. 102002. DOI: [10.1103/PhysRevD.100.102002](https://doi.org/10.1103/PhysRevD.100.102002). arXiv: [1904.00498 \[astro-ph.CO\]](https://arxiv.org/abs/1904.00498).
- [45] M. F. Albakry et al. “A Search for Low-mass Dark Matter via Bremsstrahlung Radiation and the Migdal Effect in SuperCDMS”. In: *Physical Review D* 107.11 (June 1, 2023), p. 112013. DOI: [10.1103/PhysRevD.107.112013](https://doi.org/10.1103/PhysRevD.107.112013). arXiv: [2302.09115 \[hep-ex\]](https://arxiv.org/abs/2302.09115).
- [46] J. Aalbers et al. “A Next-Generation Liquid Xenon Observatory for Dark Matter and Neutrino Physics”. In: *J. Phys. G* 50.1 (Dec. 15, 2022), p. 013001. DOI: [10.1088/1361-6471/ac841a](https://doi.org/10.1088/1361-6471/ac841a). arXiv: [2203.02309 \[physics.ins-det\]](https://arxiv.org/abs/2203.02309).
- [47] Christopher Savage et al. “Compatibility of DAMA/LIBRA Dark Matter Detection with Other Searches”. In: *Journal of Cosmology and Astroparticle Physics* 04.04 (2009), p. 010. DOI: [10.1088/1475-7516/2009/04/010](https://doi.org/10.1088/1475-7516/2009/04/010). arXiv: [0808.3607 \[astro-ph\]](https://arxiv.org/abs/0808.3607).
- [48] G. Adhikari et al. “Strong Constraints from COSINE-100 on the DAMA Dark Matter Results Using the Same Sodium Iodide Target”. In: *Science Advances* 7.46 (Nov. 2021), abk2699. DOI: [10.1126/sciadv.abk2699](https://doi.org/10.1126/sciadv.abk2699). arXiv: [2104.03537 \[hep-ex\]](https://arxiv.org/abs/2104.03537).
- [49] C. Amole, M. Ardid, I.J. Arnquist, et al. “Dark Matter Search Results from the Complete Exposure of the PICO-60  $\mathrm{C}_3\mathrm{F}_8$  Bubble Chamber”. In: *Physical Review D* 100.2 (July 10, 2019), p. 022001. DOI: [10.1103/PhysRevD.100.022001](https://doi.org/10.1103/PhysRevD.100.022001). arXiv: [1902.04031 \[astro-ph.CO\]](https://arxiv.org/abs/1902.04031).
- [50] E. Behnke et al. “Final Results of the PICASSO Dark Matter Search Experiment”. In: *Astroparticle Physics* 90 (Apr. 2017), pp. 85–92. DOI: [10.1016/j.astropartphys.2017.02.005](https://doi.org/10.1016/j.astropartphys.2017.02.005). arXiv: [1611.01499 \[hep-ex\]](https://arxiv.org/abs/1611.01499).
- [51] D.S. Akerib, S. Alsum, H.M. Araújo, et al. “Limits on Spin-Dependent WIMP-nucleon Cross Section Obtained from the Complete LUX Exposure”. In: *Physical Review Letters* 118.25 (June 23, 2017), p. 251302. DOI: [10.1103/PhysRevLett.118.251302](https://doi.org/10.1103/PhysRevLett.118.251302). arXiv: [1705.03380 \[astro-ph.CO\]](https://arxiv.org/abs/1705.03380).
- [52] Ciaran A. J. O’Hare. “Fog on the Horizon: A New Definition of the Neutrino Floor for Direct Dark Matter Searches”. In: *Physical Review Letters* 127.25 (Dec. 16, 2021), p. 251802. DOI: [10.1103/PhysRevLett.127.251802](https://doi.org/10.1103/PhysRevLett.127.251802). arXiv: [2109.03116 \[hep-ph\]](https://arxiv.org/abs/2109.03116).

- [53] Philipp Grothaus, Malcolm Fairbairn, and Jocelyn Monroe. *Directional Dark Matter Detection Beyond the Neutrino Bound*. arXiv.org. June 19, 2014. DOI: [10.1103/PhysRevD.90.055018](https://doi.org/10.1103/PhysRevD.90.055018).
- [54] Fei-Fan Lee, Guey-Lin Lin, and Yue-Lin Sming Tsai. “Constraining Dark Matter Capture and Annihilation Cross Sections by Searching for Neutrino Signature from the Earth Core”. In: *Physical Review D* 89.2 (Jan. 6, 2014), p. 025003. DOI: [10.1103/PhysRevD.89.025003](https://doi.org/10.1103/PhysRevD.89.025003). arXiv: [1308.1782 \[hep-ph\]](https://arxiv.org/abs/1308.1782).
- [55] A. Albert et al. “Search for Dark Matter Annihilation in the Earth Using the ANTARES Neutrino Telescope”. In: *Phys. Dark Univ.* 16 (June 2017), pp. 41–48. DOI: [10.1016/j.dark.2017.04.005](https://doi.org/10.1016/j.dark.2017.04.005). arXiv: [1612.06792 \[hep-ex\]](https://arxiv.org/abs/1612.06792).
- [56] H. Abdallah et al. “Search for  $\gamma$ -Ray Line Signals from Dark Matter Annihilations in the Inner Galactic Halo from 10 Years of Observations with H.E.S.S.” In: *Phys. Rev. Lett.* 120.20 (May 16, 2018), p. 201101. DOI: [10.1103/PhysRevLett.120.201101](https://doi.org/10.1103/PhysRevLett.120.201101). arXiv: [1805.05741 \[astro-ph.HE\]](https://arxiv.org/abs/1805.05741).
- [57] Alessandro Montanari and Emmanuel Moulin. “Search for Dark Matter Gamma-Ray Line Annihilation Signals in the H.E.S.S. Inner Galaxy Survey”. In: *PoS ICRC2023* (July 25, 2023), p. 1424. DOI: [10.22323/1.444.1424](https://doi.org/10.22323/1.444.1424).
- [58] F. Aharonian et al. “H.E.S.S. Observations of the Galactic Center Region and Their Possible Dark Matter Interpretation”. In: *Phys. Rev. Lett.* 97 (2006), p. 221102. DOI: [10.1103/PhysRevLett.97.221102](https://doi.org/10.1103/PhysRevLett.97.221102). arXiv: [astro-ph/0610509](https://arxiv.org/abs/astro-ph/0610509).
- [59] S. Archambault et al. “Dark Matter Constraints from a Joint Analysis of Dwarf Spheroidal Galaxy Observations with VERITAS”. In: *Phys. Rev. D* 95.8 (Apr. 5, 2017), p. 082001. DOI: [10.1103/PhysRevD.95.082001](https://doi.org/10.1103/PhysRevD.95.082001). arXiv: [1703.04937 \[astro-ph.HE\]](https://arxiv.org/abs/1703.04937).
- [60] James L. Ryan. “Search for Dark Matter Annihilation Signals in the Galactic Center Halo with VERITAS”. In: *PoS ICRC2023* (July 25, 2023), p. 794. DOI: [10.22323/1.444.0794](https://doi.org/10.22323/1.444.0794). arXiv: [2309.12403 \[astro-ph.HE\]](https://arxiv.org/abs/2309.12403).
- [61] Conor McGrath. “An Indirect Search for Dark Matter with a Combined Analysis of Dwarf Spheroidal Galaxies from VERITAS”. In: *PoS ICRC2023* (July 25, 2023), p. 1395. DOI: [10.22323/1.444.1395](https://doi.org/10.22323/1.444.1395).
- [62] J. Aleksic et al. “MAGIC Gamma-Ray Telescope Observation of the Perseus Cluster of Galaxies: Implications for Cosmic Rays, Dark Matter and NGC 1275”. In: *Astrophys. J.* 710 (2010), pp. 634–647. DOI: [10.1088/0004-637X/710/1/634](https://doi.org/10.1088/0004-637X/710/1/634). arXiv: [0909.3267 \[astro-ph.HE\]](https://arxiv.org/abs/0909.3267).

- [63] J. Aleksic et al. “Searches for Dark Matter Annihilation Signatures in the Segue 1 Satellite Galaxy with the MAGIC-I Telescope”. In: *JCAP* 06 (2011), p. 035. DOI: [10.1088/1475-7516/2011/06/035](https://doi.org/10.1088/1475-7516/2011/06/035). arXiv: [1103.0477 \[astro-ph.HE\]](https://arxiv.org/abs/1103.0477).
- [64] A. Albert et al. “Dark Matter Limits From Dwarf Spheroidal Galaxies with The HAWC Gamma-Ray Observatory”. In: *Astrophys. J.* 853.2 (Feb. 1, 2018), p. 154. DOI: [10.3847/1538-4357/aaa6d8](https://doi.org/10.3847/1538-4357/aaa6d8). arXiv: [1706.01277 \[astro-ph.HE\]](https://arxiv.org/abs/1706.01277).
- [65] A. U. Abeysekara et al. “A Search for Dark Matter in the Galactic Halo with HAWC”. In: *JCAP* 02 (Feb. 23, 2018), p. 049. DOI: [10.1088/1475-7516/2018/02/049](https://doi.org/10.1088/1475-7516/2018/02/049). arXiv: [1710.10288 \[astro-ph.HE\]](https://arxiv.org/abs/1710.10288).
- [66] Megan Longo Proper, J. Patrick Harding, and Brenda Dingus. “First Limits on the Dark Matter Cross Section with the HAWC Observatory”. In: *PoS* ICRC2015 (July 21, 2015). Ed. by Monica Tecchio and Daniel Levin, p. 1213. DOI: [10.22323/1.236.1213](https://doi.org/10.22323/1.236.1213). arXiv: [1508.04470 \[astro-ph.HE\]](https://arxiv.org/abs/1508.04470).
- [67] J. Patrick Harding and Brenda Dingus. “Dark Matter Annihilation and Decay Searches with the High Altitude Water Cherenkov (HAWC) Observatory”. In: *PoS* ICRC2015 (July 13, 2015), p. 1227. DOI: [10.22323/1.236.1227](https://doi.org/10.22323/1.236.1227). arXiv: [1508.04352 \[astro-ph.HE\]](https://arxiv.org/abs/1508.04352).
- [68] Fermi-LAT Collaboration. “Searching for Dark Matter Annihilation from Milky Way Dwarf Spheroidal Galaxies with Six Years of Fermi-LAT Data”. In: *Physical Review Letters* 115.23 (Nov. 30, 2015), p. 231301. DOI: [10.1103/PhysRevLett.115.231301](https://doi.org/10.1103/PhysRevLett.115.231301). arXiv: [1503.02641 \[astro-ph.HE\]](https://arxiv.org/abs/1503.02641).
- [69] The Fermi-LAT Collaboration. “Updated Search for Spectral Lines from Galactic Dark Matter Interactions with Pass 8 Data from the Fermi Large Area Telescope”. In: *Physical Review D* 91.12 (June 22, 2015), p. 122002. DOI: [10.1103/PhysRevD.91.122002](https://doi.org/10.1103/PhysRevD.91.122002). arXiv: [1506.00013 \[astro-ph.HE\]](https://arxiv.org/abs/1506.00013).
- [70] M. Ackermann et al. “Fermi LAT Search for Dark Matter in Gamma-ray Lines and the Inclusive Photon Spectrum”. In: *Phys. Rev. D* 86 (2012), p. 022002. DOI: [10.1103/PhysRevD.86.022002](https://doi.org/10.1103/PhysRevD.86.022002). arXiv: [1205.2739 \[astro-ph.HE\]](https://arxiv.org/abs/1205.2739).
- [71] A. A. Abdo et al. “Constraints on Cosmological Dark Matter Annihilation from the Fermi-LAT Isotropic Diffuse Gamma-Ray Measurement”. In: *JCAP* 04 (2010), p. 014. DOI: [10.1088/1475-7516/2010/04/014](https://doi.org/10.1088/1475-7516/2010/04/014). arXiv: [1002.4415 \[astro-ph.CO\]](https://arxiv.org/abs/1002.4415).
- [72] Meng Su, Tracy R. Slatyer, and Douglas P. Finkbeiner. “Giant Gamma-ray Bubbles from Fermi-LAT: AGN Activity or Bipolar Galactic Wind?” In: *Astrophys. J.* 724 (2010), pp. 1044–1082. DOI: [10.1088/0004-637X/724/2/1044](https://doi.org/10.1088/0004-637X/724/2/1044). arXiv: [1005.5480 \[astro-ph.HE\]](https://arxiv.org/abs/1005.5480).

- [73] M. G. Aartsen et al. “Search for Annihilating Dark Matter in the Sun with 3 Years of IceCube Data”. In: *Eur. Phys. J. C* 77.3 (Mar. 8, 2017), p. 146. DOI: [10.1140/epjc/s10052-017-4689-9](https://doi.org/10.1140/epjc/s10052-017-4689-9). arXiv: [1612.05949 \[astro-ph.HE\]](https://arxiv.org/abs/1612.05949).
- [74] M. G. Aartsen et al. “Search for Dark Matter Annihilations in the Sun with the 79-String IceCube Detector”. In: *Phys. Rev. Lett.* 110.13 (Mar. 28, 2013), p. 131302. DOI: [10.1103/PhysRevLett.110.131302](https://doi.org/10.1103/PhysRevLett.110.131302). arXiv: [1212.4097 \[astro-ph.HE\]](https://arxiv.org/abs/1212.4097).
- [75] S. Adrián-Martínez et al. “A Search for Secluded Dark Matter in the Sun with the ANTARES Neutrino Telescope”. In: *Journal of Cosmology and Astroparticle Physics* 05.05 (May 5, 2016), p. 016. DOI: [10.1088/1475-7516/2016/05/016](https://doi.org/10.1088/1475-7516/2016/05/016). arXiv: [1602.07000 \[hep-ex\]](https://arxiv.org/abs/1602.07000).
- [76] S. Adrian-Martinez, A. Albert, M. Andre, et al. “Limits on Dark Matter Annihilation in the Sun Using the ANTARES Neutrino Telescope”. In: *Physics Letters B* 759 (Aug. 10, 2016), pp. 69–74. DOI: [10.1016/j.physletb.2016.05.019](https://doi.org/10.1016/j.physletb.2016.05.019). arXiv: [1603.02228 \[astro-ph.HE\]](https://arxiv.org/abs/1603.02228).
- [77] The Super-Kamiokande Collaboration et al. “Search for Neutrinos from Annihilation of Captured Low-Mass Dark Matter Particles in the Sun by Super-Kamiokande”. In: *Phys. Rev. Lett.* 114.14 (Apr. 6, 2015), p. 141301. DOI: [10.1103/PhysRevLett.114.141301](https://doi.org/10.1103/PhysRevLett.114.141301). arXiv: [1503.04858 \[hep-ex\]](https://arxiv.org/abs/1503.04858).
- [78] S. Desai et al. “Search for Dark Matter WIMPs Using Upward Through-Going Muons in Super-Kamiokande”. In: *Phys. Rev. D* 70 (2004), p. 083523. DOI: [10.1103/PhysRevD.70.083523](https://doi.org/10.1103/PhysRevD.70.083523). arXiv: [hep-ex/0404025](https://arxiv.org/abs/hep-ex/0404025).
- [79] Jonathan L. Feng et al. “Testing the Dark Matter Interpretation of the DAMA/LIBRA Result with Super-Kamiokande”. In: *JCAP* 01 (2009), p. 032. DOI: [10.1088/1475-7516/2009/01/032](https://doi.org/10.1088/1475-7516/2009/01/032). arXiv: [0808.4151 \[hep-ph\]](https://arxiv.org/abs/0808.4151).
- [80] Nicole F. Bell, Matthew J. Dolan, and Sandra Robles. “Searching for Sub-GeV Dark Matter in the Galactic Centre Using Hyper-Kamiokande”. In: *JCAP* 09 (Sept. 8, 2020), p. 019. DOI: [10.1088/1475-7516/2020/09/019](https://doi.org/10.1088/1475-7516/2020/09/019). arXiv: [2005.01950 \[hep-ph\]](https://arxiv.org/abs/2005.01950).
- [81] Nicole F. Bell, Matthew J. Dolan, and Sandra Robles. “Searching for Dark Matter in the Sun Using Hyper-Kamiokande”. In: *JCAP* 11 (Nov. 5, 2021), p. 004. DOI: [10.1088/1475-7516/2021/11/004](https://doi.org/10.1088/1475-7516/2021/11/004). arXiv: [2107.04216 \[hep-ph\]](https://arxiv.org/abs/2107.04216).
- [82] Nicole F. Bell, Matthew J. Dolan, and Sandra Robles. “Dark Matter Pollution in the Diffuse Supernova Neutrino Background”. In: *JCAP* 11 (Nov. 30, 2022), p. 060. DOI: [10.1088/1475-7516/2022/11/060](https://doi.org/10.1088/1475-7516/2022/11/060). arXiv: [2205.14123 \[hep-ph\]](https://arxiv.org/abs/2205.14123).

- [83] Tarso Franarin, Malcolm Fairbairn, and Jonathan H. Davis. “JUNO Sensitivity to Resonant Absorption of Galactic Supernova Neutrinos by Dark Matter”. In: *arXiv:1806.05015 [hep-ph]* (June 2018). arXiv: [1806 . 05015 \[hep-ph\]](https://arxiv.org/abs/1806.05015).
- [84] Gaëlle Giesen et al. “AMS-02 Antiprotons, at Last! Secondary Astrophysical Component and Immediate Implications for Dark Matter”. In: *JCAP* 09 (Sept. 8, 2015), p. 023. DOI: [10 . 1088 / 1475 - 7516 / 2015 / 9 / 023](https://doi.org/10.1088/1475-7516/2015/9/023). arXiv: [1504 . 04276 \[astro-ph.HE\]](https://arxiv.org/abs/1504.04276).
- [85] Lars Bergstrom et al. “New Limits on Dark Matter Annihilation from AMS Cosmic Ray Positron Data”. In: *Phys. Rev. Lett.* 111 (Oct. 21, 2013), p. 171101. DOI: [10 . 1103 / PhysRevLett . 111 . 171101](https://doi.org/10.1103/PhysRevLett.111.171101). arXiv: [1306 . 3983 \[astro-ph.HE\]](https://arxiv.org/abs/1306.3983).
- [86] Seyda Ipek, David McKeen, and Ann E. Nelson. “A Renormalizable Model for the Galactic Center Gamma Ray Excess from Dark Matter Annihilation”. In: *Phys. Rev. D* 90.5 (Sept. 22, 2014), p. 055021. DOI: [10 . 1103 / PhysRevD . 90 . 055021](https://doi.org/10.1103/PhysRevD.90.055021). arXiv: [1404 . 3716 \[hep-ph\]](https://arxiv.org/abs/1404.3716).
- [87] M. Ackermann et al. “The Fermi Galactic Center GeV Excess and Implications for Dark Matter”. In: *Astrophys. J.* 840.1 (May 4, 2017), p. 43. DOI: [10 . 3847 / 1538 - 4357 / aa6cab](https://doi.org/10.3847/1538-4357/aa6cab). arXiv: [1704 . 03910 \[astro-ph.HE\]](https://arxiv.org/abs/1704.03910).
- [88] V. Bonnivard et al. “Dark Matter Annihilation and Decay in Dwarf Spheroidal Galaxies: The Classical and Ultrafaint dSphs”. In: *Mon. Not. Roy. Astron. Soc.* 453.1 (Oct. 11, 2015), pp. 849–867. DOI: [10 . 1093 / mnras / stv1601](https://doi.org/10.1093/mnras/stv1601). arXiv: [1504 . 02048 \[astro-ph.HE\]](https://arxiv.org/abs/1504.02048).
- [89] Haipeng An, Maxim Pospelov, and Josef Pradler. “New Stellar Constraints on Dark Photons”. In: *Phys. Lett. B* 725 (Oct. 1, 2013), pp. 190–195. DOI: [10 . 1016 / j . physletb . 2013 . 07 . 008](https://doi.org/10.1016/j.physletb.2013.07.008). arXiv: [1302 . 3884 \[hep-ph\]](https://arxiv.org/abs/1302.3884).
- [90] Matthew J. Dolan, Frederick J. Hiskens, and Raymond R. Volkas. “Advancing Globular Cluster Constraints on the Axion-Photon Coupling”. In: *JCAP* 10 (Oct. 31, 2022), p. 096. DOI: [10 . 1088 / 1475 - 7516 / 2022 / 10 / 096](https://doi.org/10.1088/1475-7516/2022/10/096). arXiv: [2207 . 03102 \[hep-ph\]](https://arxiv.org/abs/2207.03102).
- [91] Matthew J. Dolan, Frederick J. Hiskens, and Raymond R. Volkas. “Constraining Dark Photons with Self-consistent Simulations of Globular Cluster Stars”. In: *arXiv:2306.13335 [hep-ph]* (June 2023). arXiv: [2306 . 13335 \[hep-ph\]](https://arxiv.org/abs/2306.13335).
- [92] W. H. Press and D. N. Spergel. “Capture by the Sun of a Galactic Population of Weakly Interacting, Massive Particles”. In: *The Astrophysical Journal* 296 (1985), pp. 679–684. DOI: [10 . 1086 / 163485](https://doi.org/10.1086/163485).

- [93] Andrew Gould. “Weakly Interacting Massive Particle Distribution in and Evaporation from the Sun”. In: *The Astrophysical Journal* 321 (1987), p. 560. DOI: [10.1086/165652](https://doi.org/10.1086/165652).
- [94] Andrew Gould. “Resonant Enhancements in WIMP Capture by the Earth”. In: *Astrophys. J.* 321 (1987), p. 571. DOI: [10.1086/165653](https://doi.org/10.1086/165653).
- [95] Giorgio Busoni et al. “Evaporation and Scattering of Momentum- and Velocity-Dependent Dark Matter in the Sun”. In: *Journal of Cosmology and Astroparticle Physics* 10.10 (Oct. 23, 2017), p. 037. DOI: [10.1088/1475-7516/2017/10/037](https://doi.org/10.1088/1475-7516/2017/10/037). arXiv: [1703.07784 \[hep-ph\]](https://arxiv.org/abs/1703.07784).
- [96] Andrew Gould. “Big Bang Archeology: WIMP Capture by the Earth at Finite Optical Depth”. In: *Astrophys. J.* 387 (1992), p. 21. DOI: [10.1086/171057](https://doi.org/10.1086/171057).
- [97] Raghuveer Garani and Sergio Palomares-Ruiz. “Dark Matter in the Sun: Scattering off Electrons vs Nucleons”. In: *JCAP* 05 (May 3, 2017), p. 007. DOI: [10.1088/1475-7516/2017/05/007](https://doi.org/10.1088/1475-7516/2017/05/007). arXiv: [1702.02768 \[hep-ph\]](https://arxiv.org/abs/1702.02768).
- [98] Joseph Bramante, Antonio Delgado, and Adam Martin. “Multiscatter Stellar Capture of Dark Matter”. In: *Phys. Rev. D* 96.6 (Sept. 6, 2017), p. 063002. DOI: [10.1103/PhysRevD.96.063002](https://doi.org/10.1103/PhysRevD.96.063002). arXiv: [1703.04043 \[hep-ph\]](https://arxiv.org/abs/1703.04043).
- [99] The Super-Kamiokande Collaboration et al. “An Indirect Search for WIMPs in the Sun Using 3109.6 Days of Upward-Going Muons in Super-Kamiokande”. In: *The Astrophysical Journal* 742.2 (2011), p. 78. DOI: [10.1088/0004-637X/742/2/78](https://doi.org/10.1088/0004-637X/742/2/78). arXiv: [1108.3384 \[astro-ph.HE\]](https://arxiv.org/abs/1108.3384).
- [100] M. G. Aartsen et al. “Search for Annihilating Dark Matter in the Sun with 3 Years of IceCube Data”. In: *Eur. Phys. J.* C77.3 (2017), p. 146. DOI: [10.1140/epjc/s10052-019-6702-y](https://doi.org/10.1140/epjc/s10052-019-6702-y), [10.1140/epjc/s10052-017-4689-9](https://doi.org/10.1140/epjc/s10052-017-4689-9). arXiv: [1612.05949 \[astro-ph.HE\]](https://arxiv.org/abs/1612.05949).
- [101] Brian Batell et al. “Solar Gamma Rays Powered by Secluded Dark Matter”. In: *Physical Review D* 81.7 (2010), p. 075004. DOI: [10.1103/PhysRevD.81.075004](https://doi.org/10.1103/PhysRevD.81.075004). arXiv: [0910.1567 \[hep-ph\]](https://arxiv.org/abs/0910.1567).
- [102] Philip Schuster, Natalia Toro, and Itay Yavin. “Terrestrial and Solar Limits on Long-Lived Particles in a Dark Sector”. In: *Physical Review D* 81.1 (2010), p. 016002. DOI: [10.1103/PhysRevD.81.016002](https://doi.org/10.1103/PhysRevD.81.016002). arXiv: [0910.1602 \[hep-ph\]](https://arxiv.org/abs/0910.1602).
- [103] Nicole F. Bell and Kalliopi Petraki. “Enhanced Neutrino Signals from Dark Matter Annihilation in the Sun via Metastable Mediators”. In: *Journal of Cosmology and Astroparticle Physics* 04.04 (2011), p. 003. DOI: [10.1088/1475-7516/2011/04/003](https://doi.org/10.1088/1475-7516/2011/04/003). arXiv: [1102.2958 \[hep-ph\]](https://arxiv.org/abs/1102.2958).

- [104] Jonathan L. Feng, Jordan Smolinsky, and Philip Tanedo. “Dark Sunshine: Detecting Dark Matter through Dark Photons from the Sun”. In: *Physical Review D* 93.11 (June 28, 2016), p. 115036. DOI: [10.1103/PhysRevD.93.115036](https://doi.org/10.1103/PhysRevD.93.115036). arXiv: [1602.01465 \[hep-ph\]](https://arxiv.org/abs/1602.01465).
- [105] Rebecca K. Leane, Kenny C. Y. Ng, and John F. Beacom. “Powerful Solar Signatures of Long-Lived Dark Mediators”. In: *Physical Review D* 95.12 (June 29, 2017), p. 123016. DOI: [10.1103/PhysRevD.95.123016](https://doi.org/10.1103/PhysRevD.95.123016). arXiv: [1703.04629 \[astro-ph.HE\]](https://arxiv.org/abs/1703.04629).
- [106] Andrew Gould and Georg Raffelt. “THERMAL CONDUCTION BY MASSIVE PARTICLES”. In: *Astrophys. J.* 352 (1990), p. 654. DOI: [10.1086/168568](https://doi.org/10.1086/168568).
- [107] Andrew Gould and Georg Raffelt. “Cosmion Energy Transfer in Stars: The Knudsen Limit”. In: *The Astrophysical Journal* 352 (1990), p. 669. DOI: [10.1086/168569](https://doi.org/10.1086/168569).
- [108] Aaron C. Vincent and Pat Scott. “Thermal Conduction by Dark Matter with Velocity and Momentum-Dependent Cross-Sections”. In: *Journal of Cosmology and Astroparticle Physics* 04.04 (Apr. 22, 2014), p. 019. DOI: [10.1088/1475-7516/2014/04/019](https://doi.org/10.1088/1475-7516/2014/04/019). arXiv: [1311.2074 \[astro-ph.CO\]](https://arxiv.org/abs/1311.2074).
- [109] Ben Geytenbeek et al. “Effect of Electromagnetic Dipole Dark Matter on Energy Transport in the Solar Interior”. In: *Journal of Cosmology and Astroparticle Physics* 03.03 (Mar. 13, 2017), p. 029. DOI: [10.1088/1475-7516/2017/03/029](https://doi.org/10.1088/1475-7516/2017/03/029). arXiv: [1610.06737 \[hep-ph\]](https://arxiv.org/abs/1610.06737).
- [110] Samuel D. McDermott, Hai-Bo Yu, and Kathryn M. Zurek. “Constraints on Scalar Asymmetric Dark Matter from Black Hole Formation in Neutron Stars”. In: *Phys. Rev. D* 85 (2012), p. 023519. DOI: [10.1103/PhysRevD.85.023519](https://doi.org/10.1103/PhysRevD.85.023519). arXiv: [1103.5472 \[hep-ph\]](https://arxiv.org/abs/1103.5472).
- [111] Chris Kouvaris and Peter Tinyakov. “Excluding Light Asymmetric Bosonic Dark Matter”. In: *Phys. Rev. Lett.* 107 (2011), p. 091301. DOI: [10.1103/PhysRevLett.107.091301](https://doi.org/10.1103/PhysRevLett.107.091301). arXiv: [1104.0382 \[astro-ph.CO\]](https://arxiv.org/abs/1104.0382).
- [112] Tolga Güver et al. “On the Capture of Dark Matter by Neutron Stars”. In: *JCAP* 05 (May 13, 2014), p. 013. DOI: [10.1088/1475-7516/2014/05/013](https://doi.org/10.1088/1475-7516/2014/05/013). arXiv: [1201.2400 \[hep-ph\]](https://arxiv.org/abs/1201.2400).
- [113] Raghubeer Garani, Yoann Genolini, and Thomas Hambye. “New Analysis of Neutron Star Constraints on Asymmetric Dark Matter”. In: *JCAP* 05 (May 21, 2019), p. 035. DOI: [10.1088/1475-7516/2019/05/035](https://doi.org/10.1088/1475-7516/2019/05/035). arXiv: [1812.08773 \[hep-ph\]](https://arxiv.org/abs/1812.08773).

- [114] Joseph Bramante et al. “Bounds on Self-Interacting Fermion Dark Matter from Observations of Old Neutron Stars”. In: *Phys. Rev. D* 89.1 (Jan. 21, 2014), p. 015010. DOI: [10.1103/PhysRevD.89.015010](https://doi.org/10.1103/PhysRevD.89.015010). arXiv: [1310.3509 \[hep-ph\]](https://arxiv.org/abs/1310.3509).
- [115] Bridget Bertoni, Ann E. Nelson, and Sanjay Reddy. “Dark Matter Thermalization in Neutron Stars”. In: *Phys. Rev. D* 88 (Dec. 3, 2013), p. 123505. DOI: [10.1103/PhysRevD.88.123505](https://doi.org/10.1103/PhysRevD.88.123505). arXiv: [1309.1721 \[hep-ph\]](https://arxiv.org/abs/1309.1721).
- [116] Nicole F. Bell, Andrew Melatos, and Kalliopi Petraki. “Realistic Neutron Star Constraints on Bosonic Asymmetric Dark Matter”. In: *Phys. Rev. D* 87.12 (June 7, 2013), p. 123507. DOI: [10.1103/PhysRevD.87.123507](https://doi.org/10.1103/PhysRevD.87.123507). arXiv: [1301.6811 \[hep-ph\]](https://arxiv.org/abs/1301.6811).
- [117] Joseph Bramante, Tim Linden, and Yu-Dai Tsai. “Searching for Dark Matter with Neutron Star Mergers and Quiet Kilonovae”. In: *Physical Review D* 97.5 (Mar. 12, 2018), p. 055016. DOI: [10.1103/PhysRevD.97.055016](https://doi.org/10.1103/PhysRevD.97.055016). arXiv: [1706.00001 \[hep-ph\]](https://arxiv.org/abs/1706.00001).
- [118] John Ellis et al. “Search for Dark Matter Effects on Gravitational Signals from Neutron Star Mergers”. In: *Physics Letters B* 781 (June 10, 2018), pp. 607–610. DOI: [10.1016/j.physletb.2018.04.048](https://doi.org/10.1016/j.physletb.2018.04.048). arXiv: [1710.05540 \[astro-ph.CO\]](https://arxiv.org/abs/1710.05540).
- [119] John Ellis et al. “Dark Matter Effects On Neutron Star Properties”. In: *Physical Review D* 97.12 (June 15, 2018), p. 123007. DOI: [10.1103/PhysRevD.97.123007](https://doi.org/10.1103/PhysRevD.97.123007). arXiv: [1804.01418 \[astro-ph.CO\]](https://arxiv.org/abs/1804.01418).
- [120] Ann Nelson, Sanjay Reddy, and Dake Zhou. “Dark Halos around Neutron Stars and Gravitational Waves”. In: *Journal of Cosmology and Astroparticle Physics* 07.07 (July 4, 2019), p. 012. DOI: [10.1088/1475-7516/2019/07/012](https://doi.org/10.1088/1475-7516/2019/07/012). arXiv: [1803.03266 \[hep-ph\]](https://arxiv.org/abs/1803.03266).
- [121] Heinrich Steigerwald et al. “Dark Matter Thermonuclear Supernova Ignition”. In: *arXiv:1912.12417 [astro-ph.HE]* (Dec. 2019). arXiv: [1912.12417 \[astro-ph.HE\]](https://arxiv.org/abs/1912.12417).
- [122] Grigoris Panotopoulos and Ilídio Lopes. “Constraints on Light Dark Matter Particles Using White Dwarf Stars”. In: *International Journal of Modern Physics D* 29.08 (June 3, 2020), p. 2050058. DOI: [10.1142/S0218271820500583](https://doi.org/10.1142/S0218271820500583). arXiv: [2005.11563 \[hep-ph\]](https://arxiv.org/abs/2005.11563).
- [123] Matthew McCullough and Malcolm Fairbairn. “Capture of Inelastic Dark Matter in White Dwarves”. In: *Physical Review D* 81.8 (2010), p. 083520. DOI: [10.1103/PhysRevD.81.083520](https://doi.org/10.1103/PhysRevD.81.083520). arXiv: [1001.2737 \[hep-ph\]](https://arxiv.org/abs/1001.2737).

- [124] Dan Hooper et al. “Inelastic Dark Matter As An Efficient Fuel For Compact Stars”. In: *Physical Review D* 81.10 (2010), p. 103531. DOI: [10.1103/PhysRevD.81.103531](https://doi.org/10.1103/PhysRevD.81.103531). arXiv: [1002.0005 \[hep-ph\]](https://arxiv.org/abs/1002.0005).
- [125] Joseph Bramante. “Dark Matter Ignition of Type Ia Supernovae”. In: *Phys. Rev. Lett.* 115.14 (Sept. 29, 2015), p. 141301. DOI: [10.1103/PhysRevLett.115.141301](https://doi.org/10.1103/PhysRevLett.115.141301). arXiv: [1505.07464 \[hep-ph\]](https://arxiv.org/abs/1505.07464).
- [126] Gianfranco Bertone and Malcolm Fairbairn. “Compact Stars as Dark Matter Probes”. In: *Physical Review D* 77.4 (2008), p. 043515. DOI: [10.1103/PhysRevD.77.043515](https://doi.org/10.1103/PhysRevD.77.043515). arXiv: [0709.1485 \[astro-ph\]](https://arxiv.org/abs/0709.1485).
- [127] Nirmal Raj, Philip Tanedo, and Hai-Bo Yu. “Neutron Stars at the Dark Matter Direct Detection Frontier”. In: *Physical Review D* 97.4 (Feb. 10, 2018), p. 043006. DOI: [10.1103/PhysRevD.97.043006](https://doi.org/10.1103/PhysRevD.97.043006). arXiv: [1707.09442 \[hep-ph\]](https://arxiv.org/abs/1707.09442).
- [128] Masha Baryakhtar et al. “Dark Kinetic Heating of Neutron Stars and An Infrared Window On WIMPs, SIMPs, and Pure Higgsinos”. In: *Physical Review Letters* 119.13 (Sept. 26, 2017), p. 131801. DOI: [10.1103/PhysRevLett.119.131801](https://doi.org/10.1103/PhysRevLett.119.131801). arXiv: [1704.01577 \[hep-ph\]](https://arxiv.org/abs/1704.01577).
- [129] Nicole F. Bell, Giorgio Busoni, and Sandra Robles. “Heating up Neutron Stars with Inelastic Dark Matter”. In: *JCAP* 09 (Sept. 10, 2018), p. 018. DOI: [10.1088/1475-7516/2018/09/018](https://doi.org/10.1088/1475-7516/2018/09/018). arXiv: [1807.02840 \[hep-ph\]](https://arxiv.org/abs/1807.02840).
- [130] Aniket Joglekar et al. “Relativistic Capture of Dark Matter by Electrons in Neutron Stars”. In: *Phys. Lett. B* 809 (Sept. 4, 2020), p. 135767. DOI: [10.1016/j.physletb.2020.135767](https://doi.org/10.1016/j.physletb.2020.135767). arXiv: [1911.13293 \[hep-ph\]](https://arxiv.org/abs/1911.13293).
- [131] Javier F. Acevedo et al. “Warming Nuclear Pasta with Dark Matter: Kinetic and Annihilation Heating of Neutron Star Crusts”. In: *JCAP* 03 (Mar. 17, 2020), p. 038. DOI: [10.1088/1475-7516/2020/03/038](https://doi.org/10.1088/1475-7516/2020/03/038). arXiv: [1911.06334 \[hep-ph\]](https://arxiv.org/abs/1911.06334).
- [132] Nicole F. Bell, Giorgio Busoni, and Sandra Robles. “Capture of Leptophilic Dark Matter in Neutron Stars”. In: *JCAP* 06 (June 28, 2019), p. 054. DOI: [10.1088/1475-7516/2019/06/054](https://doi.org/10.1088/1475-7516/2019/06/054). arXiv: [1904.09803 \[hep-ph\]](https://arxiv.org/abs/1904.09803).
- [133] Raghuveer Garami and Julian Heeck. “Dark Matter Interactions with Muons in Neutron Stars”. In: *Phys. Rev. D* 100.3 (Aug. 31, 2019), p. 035039. DOI: [10.1103/PhysRevD.100.035039](https://doi.org/10.1103/PhysRevD.100.035039). arXiv: [1906.10145 \[hep-ph\]](https://arxiv.org/abs/1906.10145).
- [134] Shiuli Chatterjee et al. “Faint Light of Old Neutron Stars and Detectability at the James Webb Space Telescope”. In: *Phys. Rev. D* 108.2 (July 11, 2023), p. L021301. DOI: [10.1103/PhysRevD.108.L021301](https://doi.org/10.1103/PhysRevD.108.L021301). arXiv: [2205.05048 \[astro-ph.HE\]](https://arxiv.org/abs/2205.05048).

- 
- [135] Richard C. Tolman. “Static Solutions of Einstein’s Field Equations for Spheres of Fluid”. In: *Physical Review* 55.4 (1939), pp. 364–373. DOI: [10.1103/PhysRev.55.364](https://doi.org/10.1103/PhysRev.55.364).
  - [136] J. R. Oppenheimer and G. M. Volkoff. “On Massive Neutron Cores”. In: *Physical Review* 55.4 (1939), pp. 374–381. DOI: [10.1103/PhysRev.55.374](https://doi.org/10.1103/PhysRev.55.374).
  - [137] G. Fontaine, P. Brassard, and P. Bergeron. “The Potential of White Dwarf Cosmochronology”. In: *Publications of the Astronomical Society of the Pacific* 113.782 (Apr. 2001), pp. 409–435. DOI: [10.1086/319535](https://doi.org/10.1086/319535).
  - [138] E. E. Salpeter. “Energy and Pressure of a Zero-Temperature Plasma.” In: *Astrophysical Journal* 134 (Nov. 1961), p. 669. DOI: [10.1086/147194](https://doi.org/10.1086/147194).
  - [139] R.P. Feynman, N. Metropolis, and E. Teller. “Equations of State of Elements Based on the Generalized Fermi-Thomas Theory”. In: *Physical Review* 75 (1949), pp. 1561–1573. DOI: [10.1103/PhysRev.75.1561](https://doi.org/10.1103/PhysRev.75.1561).
  - [140] M. Rotondo et al. “On the Relativistic Thomas-Fermi Treatment of Compressed Atoms and Compressed Nuclear Matter Cores of Stellar Dimensions”. In: *Physical Review C: Nuclear Physics* 83 (2011), p. 045805. DOI: [10.1103/PhysRevC.83.045805](https://doi.org/10.1103/PhysRevC.83.045805). arXiv: [0911.4622 \[astro-ph.SR\]](https://arxiv.org/abs/0911.4622).
  - [141] Michael Rotondo et al. “The Relativistic Feynman-Metropolis-Teller Theory for White Dwarfs in General Relativity”. In: *Phys. Rev. D* 84 (2011), p. 084007. DOI: [10.1103/PhysRevD.84.084007](https://doi.org/10.1103/PhysRevD.84.084007). arXiv: [1012.0154 \[astro-ph.SR\]](https://arxiv.org/abs/1012.0154).
  - [142] S.M. de Carvalho et al. “Relativistic Feynman-Metropolis-Teller Treatment at Finite Temperatures”. In: *Int. J. Mod. Phys. Conf. Ser.* 23 (2013), p. 244. DOI: [10.1103/PhysRevC.89.015801](https://doi.org/10.1103/PhysRevC.89.015801). arXiv: [1312.2434 \[astro-ph.SR\]](https://arxiv.org/abs/1312.2434).
  - [143] Nicola Pietro Gentile Fusillo et al. “A Gaia Data Release 2 Catalogue of White Dwarfs and a Comparison with SDSS”. In: *Mon. Not. Roy. Astron. Soc.* 482.4 (Feb. 2019), pp. 4570–4591. DOI: [10.1093/mnras/sty3016](https://doi.org/10.1093/mnras/sty3016). arXiv: [1807.03315 \[astro-ph.SR\]](https://arxiv.org/abs/1807.03315).
  - [144] Chris Kouvaris. “WIMP Annihilation and Cooling of Neutron Stars”. In: *Physical Review D* 77.2 (2008), p. 023006. DOI: [10.1103/PhysRevD.77.023006](https://doi.org/10.1103/PhysRevD.77.023006). arXiv: [0708.2362 \[astro-ph\]](https://arxiv.org/abs/0708.2362).